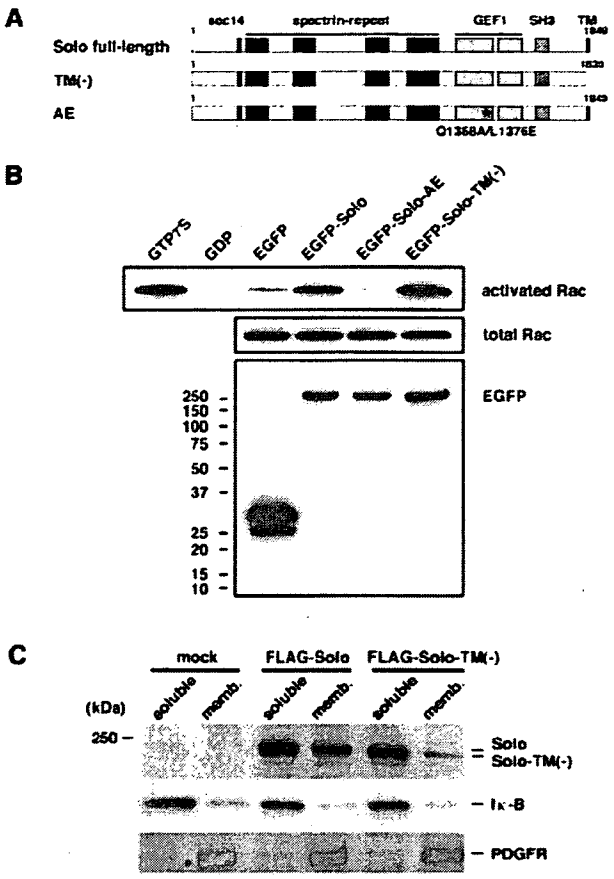

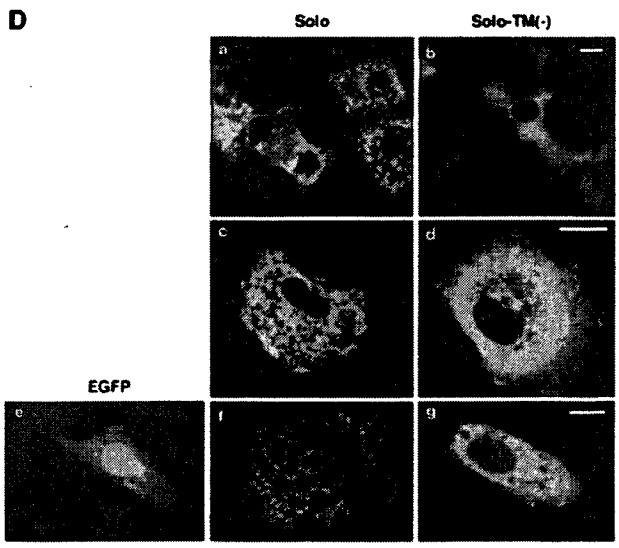

FIG. 3. GEF activity of Solo/Trio8 and localization in cellular membranes. (A) Schematic representation of full-length, C-terminally truncated Solo-TM(−) and AE mutant (GEF inactive; Q1368A/L1376E). (B) Rac1 activation by the GEF1 activity of Solo/Trio8. EGFP, EGFP-Solo, EGFP–Solo-AE, and EGFP–Solo-TM(−) were transiently expressed in COS-7 cells. Cells were cultured for 24 h and then serum starved for an additional 5 h prior to the Rac1 activation assay. PBD-bound Rac1 protein was pulled down and analyzed by Western blotting with monoclonal anti-Rac1. (Top) GTP-bound Rac1 (active form). Cell lysates treated with GTPγS or GDP served as the respective positive and negative controls. (Middle) Total cell lysates probed for Rac1 demonstrate equal amounts of total Rac1 in all transfected cells. (Bottom) Expression of transfected proteins was evaluated by Western blotting with anti-GFP. The values on the left are molecular sizes in kilodaltons. (C) COS-7 cells were transfected with pCI-neo (mock), pCI-neo-FLAG-Solo, or pCI-neo-FLAG-Solo-TM(−). Soluble and membrane proteins were subjected to sodium dodecyl sulfate-polyacrylamide gel electrophoresis and immunoblotted with anti-FLAG, anti-Iκ-B (soluble-protein control), or anti-PDGF-Rα/β (membrane protein control). (D) Fluorescence microscopy of cells transfected with N- or C-terminally EGFP- or FLAG-tagged Solo or C-terminally truncated Solo-TM(−) expression constructs. Expression constructs encoding N-terminally EGFP-tagged Solo and Solo-TM(−) were transfected into COS-7 cells (a, b). Expression constructs of C-terminally FLAG-tagged Solo and Solo-TM(−) were transfected into COS-7 cells and stained with anti-FLAG (c, d). EGFP alone, C-terminally EGFP-tagged Solo, and Solo-TM(−) mutant expression constructs were transfected into NIH 3T3 cells (e to g). Bars = 10 μm.

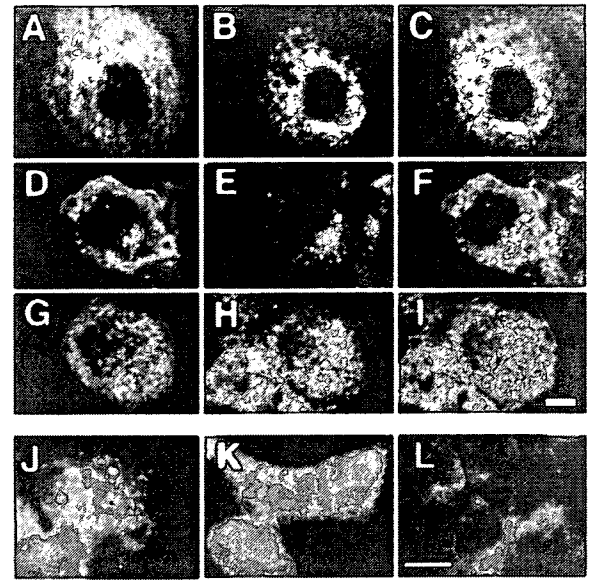

FIG. 4. Subcellular localization of Solo/Trio8. An EGFP-tagged Solo/Trio8 expression construct (green) was transfected into COS-7 cells (A, D, and G). COS-7 cells were further stained (red) with anti-Bip/GRP78 (B), anti-GM130 (E), or anti-EEA1 (H). Merged images are indicated to the right in each row (C, F, and I). Images were obtained by confocal microscopy. The EGFP-tagged Solo/Trio8 expression construct was transfected into 293 cells, and EGFP staining (green) was assessed. The 293 cells were further stained (red) for specific markers with anti-Rab5a (J), anti-Rab7 (K), or anti-Rab11 (L). Merged images are indicated, and colocalization is shown in yellow (blue arrowheads in J). Images were obtained with a charge-coupled device camera. Bars = 5 μm.

Solo-AE, or EGFP–Solo-TM(−) expression construct (Fig. 3B, middle). Furthermore, the amount of EGFP-Solo did not differ between COS-7 cells transfected with WT or mutant Solo constructs (Fig. 3B, bottom).

Solo/Trio8 localizes to early endosomes. To address whether the potential C-terminal membrane-anchoring domain of Solo/Trio8 is required for membrane association, N-terminally FLAG-tagged Solo and Solo-TM(−) expression constructs (Fig. 3A) were transfected into COS-7 cells and the cell lysates

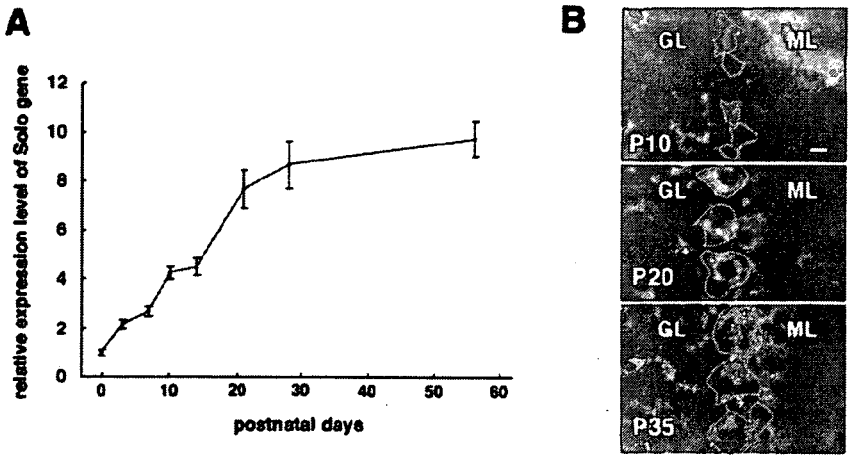

FIG. 5. Expression profile of Solo/Trio8 and the increase in the number of early endosomes during postnatal mouse cerebellar development. (A) SYBR green-based quantitative RT-PCR analysis of Solo/Trio8 transcript in WT mouse cerebellum during postnatal development. Expression levels are relative to P0 (P0 = 1.0). Each bar represents the mean ± the standard error of the mean (n = 3; three cerebella). (B) Immunohistochemistry of cerebellum sections during stages of postnatal maturation of Purkinje neurons (P10, P20, and P35). A section (20 μm) was obtained from a C57BL/6J mouse brain. Sections were stained with anti-calbindin and coimmunostained with anti-EEA1. Merged images are shown in gray. Green lines indicate the location of each cell body of calbindin-positive Purkinje neurons. Bright, dot-like signals indicate EEA1-positive early endosomes. GL, granule cell layer; ML, molecular cell layer. Bar = 20 μm

were analyzed by Western blotting. N-terminally FLAG-tagged Solo was a single band of ~220 kDa that localized to both soluble and membrane fractions (Fig. 3C). Nearly all of the N-terminally FLAG-tagged Solo-TM(−) was found in the soluble fraction (Fig. 3C), indicating that the C-terminal domain is essential for membrane anchoring. The internal control proteins IκB (soluble) and PDGF receptor α/β (membrane associated) were detected in the appropriate fractions (Fig. 3C). The subcellular localization of Solo was confirmed by immunofluorescence microscopy of N- or C-terminally EGFP- or FLAG-tagged Solo constructs. The N-terminally tagged construct displayed a pattern consistent with localization to the cytoplasm and to small vesicles in COS-7 cells (Fig. 3D, a; Fig. 4A, D, and G), 293 cells (Fig. 4J to L), and primary cultured neurons (see Fig. 7D). The C-terminally tagged protein yielded similar results (Fig. 3D, c, COS-7; Fig. 3D, f, NIH 3T3). N-terminally and C-terminally EGFP- or FLAG-tagged Solo-TM(−) displayed uniform cytoplasmic localization (Fig. 3D, b, d, and g). These results indicated that the putative C-terminal membrane-anchoring domain is essential for vesicular localization. Although various N-terminally truncated Solo mutant constructs generated by serial deletion of N-terminal domains, including the sec14-like and spectrin-repeat domains, also failed to distribute to vesicles, Western blotting revealed that these mutant proteins were not stable in COS-7 cells (data not shown).

Subcellular localization of Solo/Trio8 was then analyzed with organelle-specific markers. Antibodies against Bip/GRP78, GM130, and EEA1 specifically label the endoplasmic reticulum (22, 31), Golgi (1), and early endosomes (5, 9), respectively (Fig. 4B, E, and H). Of these markers, only the signal for the early-endosome marker EEA1 partially overlapped the EGFP-Solo signal (Fig. 4A to I), suggesting that Solo/Trio8 localizes to early endosomes. To confirm the localization with other endosomal markers and another cell type, we stained EGFP-Solo-expressing 293 cells with specific antibodies to Rab5 for early endosomes (28), Rab7 for late endosomes (11), and Rab11 for recycling endosomes (40). EGFP-Solo staining partially overlapped Rab5-positive vesicles (Fig. 4J) but not Rab7- or Rab11-positive vesicles (Fig. 4K and L). These data indicated that Solo/Trio8 localizes to early endosomes. However, at this level of resolution, we could not rule out the possibility that the observed colocalization of Solo with EEA1 and Rab5 arose from coincidental overlap due to the high-density punctate staining resulting from overexpression of these proteins.

We could not define which subclass of early endosomes expressed Solo/Trio8 because specific markers for such a classification are not available.

Solo/Trio8 gene expression correlates with early-endosome maturation levels in postnatal Purkinje neuronal cells. We analyzed the temporal pattern of the Solo/Trio8 gene expression level during Purkinje neuron maturation after birth (Fig. 5A). Analysis of mRNA samples prepared from P0 to P56 cerebella showed that the gene for Solo/Trio8 was expressed after birth, markedly increased during the first 4 weeks of life, and achieved maximal levels during adulthood. To investigate the development of early endosomes in Purkinje neurons, we stained cerebellar brain sections with antibodies against EEA1 and calbindin D28k (Purkinje neuron marker) (34). The number of large EEA1-positive early endosomes increased in Purkinje neurons during the postnatal maturation stage after P20 (Fig. 5B), indicating a correlation between expression levels of Solo/Trio8 and early-endosome development in D28k-positive Purkinje neurons.

Solo/Trio8 modulates early-endosome dynamics via its GEF1 activity and C-terminal membrane-anchoring domain. We assessed the effect of Solo overexpression on EEA1-positive early endosomes in COS-7 cells. The average number of EEA1-positive early endosomes increased in EGFP-Solo-expressing cells (1.84-fold ± 0.217-fold versus EGFP alone; $P <$ 0.001, n = 40; Fig. 6A and B). We next addressed whether

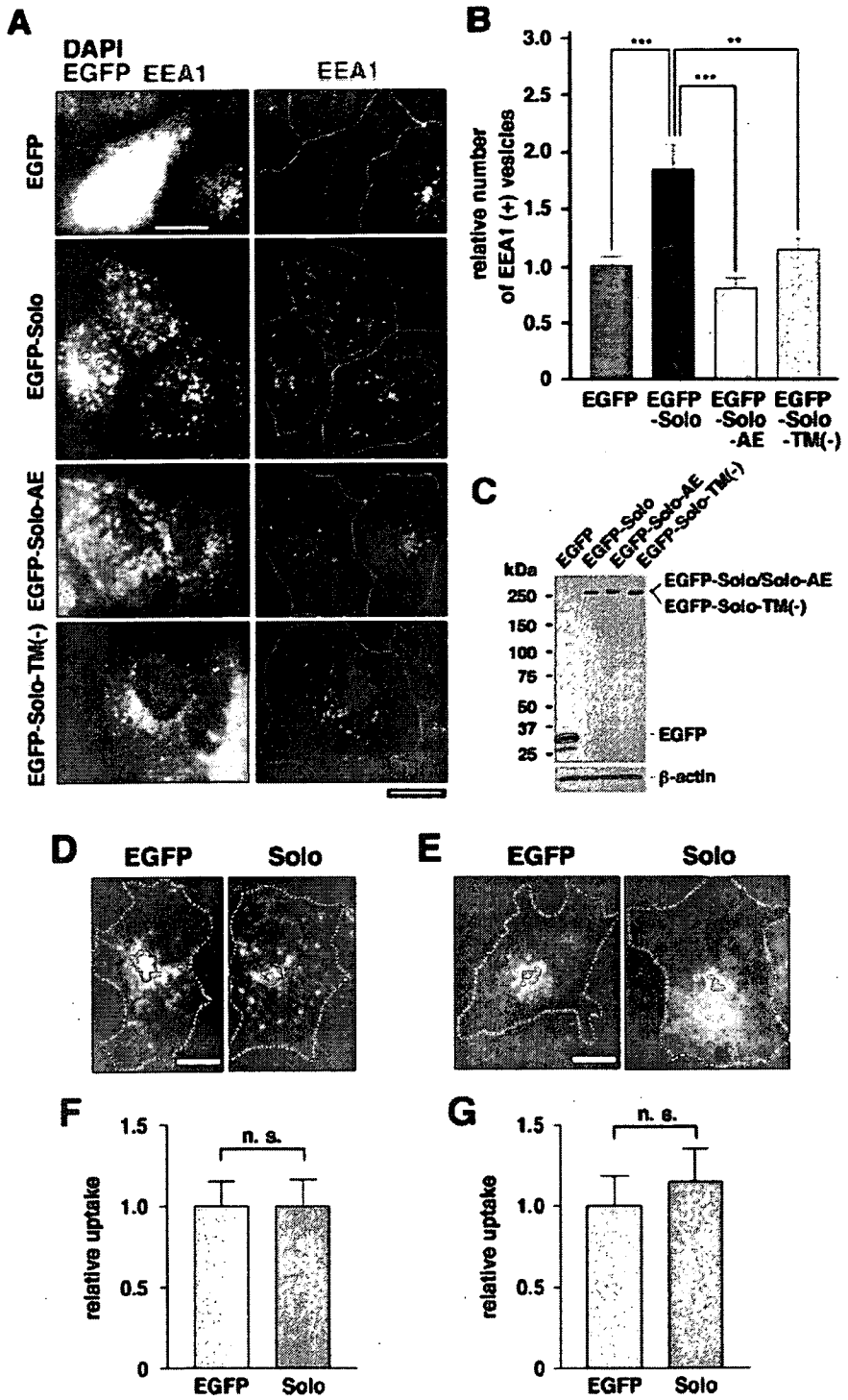

FIG. 6. Solo/Trio8 modulates early-endosome dynamics. (A) Expression constructs of the control EGFP, EGFP-Solo, EGFP–Solo-AE (GEF1 inactive form), and EGFP-Solo-TM(−) were transfected into COS-7 cells (EGFP signal is indicated in green). At 8 h posttransfection, cells were stained with anti-EEA1 (red) and DAPI (blue). Merged tricolor images are shown to the left. For ease of visualization, two-color images (minus the green EGFP signal) are shown to the right. Dotted lines indicate cellular edges. Images were obtained with a cooled charge-coupled device camera. Bars = 10 μm. (B) Quantification of EEA1-positive vesicles (early endosomes; survey square, >0.04 μm^2) in COS-7 cells transfected with Solo/Trio8 expression constructs. The number of early endosomes counted for each construct is presented relative to that determined for EGFP-expressing cells (negative control; EGFP = 1.0). Each bar represents the mean ± the standard error of the mean (n = 40 cells for each construct). **, $P < 0.01$; ***, $P < 0.001$. (C) Protein expression levels of EGFP (negative control), EGFP-Solo, EGFP–Solo-AE, and EGFP–Solo-TM(−) constructs were analyzed by Western blotting (8 μg protein per lane) with anti-Living Colors A.v. for EGFP detection. β-Actin expression was monitored as an internal control. (D to G) Effect of Solo/Trio8 on endocytosis. COS-7 cells expressing EGFP or EGFP-Solo were

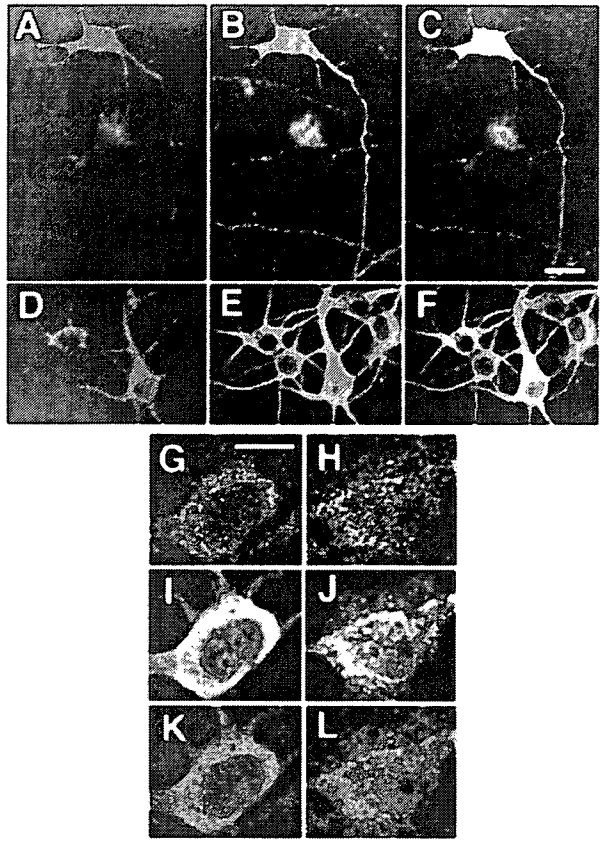

FIG. 7. Subcellular localization of Solo/Trio8 in cultured cortical neurons transfected with the EGFP-tagged Solo expression construct. EGFP signal (green) was observed in axons (A) and dendrites (D). These same cells were stained with anti-Tau1 (B) and anti-Map2 (E). Merged images are indicated to the right in each row (C and F). Images were obtained by confocal microscopy. Bar in panel C = 20 μm (same scale for panels A to F). (G to L) Cultured cortical neurons transfected with the EGFP (I) or EGFP-tagged Solo (J) expression construct. These same cells were stained with anti-Rab5a (G and H). Merged images are indicated in the lower panels (K, EGFP and Rab5a; L, EGFP-Solo and Rab5a). Bar in panel G = 10 μm (same scale for panels G to L).

GEF1 activity is required to induce the increase in EEA1-positive early endosomes with the double mutant Solo-AE (Fig. 3A), which lacks guanine nucleotide exchange activity for Rac1 (Fig. 3B). The endosome-inducing activity of this mutant was compared with that of EGFP-Solo. As expected, expression of EGFP–Solo-AE did not increase the number of EEA1-positive early endosomes (Fig. 6A and B). However, the lack of GEF1 activity altered the early-endosomal location of Solo/Trio8 (Fig. 6A). On the other hand, the distribution pattern of Solo-AE resembled that expected for lysosomal membranes, suggesting that the GEF1 activity is involved in selective transfer of Solo/Trio8 from early endosomes to late endosomes-lysosomes. Given that the Solo membrane-anchoring domain is required for membrane localization (Fig. 3C and D), we further addressed whether this domain is required to induce an increase in the number of EEA1-positive endosomes. The truncated mutant Solo-TM(−) did not increase the number of EEA1-positive endosomes (Fig. 6A and B). On the other hand, EGFP-Solo did not significantly affect the size of individual EEA1-positive early endosomes relative to EGFP-Solo mutants (data not shown). Western blotting and immunofluorescence microscopy of EGFP-derived signals in COS-7 cells confirmed that the expression levels and integrity of EGFP–Solo-AE and EGFP–Solo-TM(−) were similar to those of EGFP-Solo (Fig. 6A and C). To probe the mechanism of the Solo/Trio8-induced increase in early endosomes, we investigated the effect of Solo/Trio8 expression on endocytosis in COS-7 cells. The uptake of Alexa Fluor 594-labeled human transferrin and Sulforhodamine 101 did not change in EGFP-Solo-transfected COS-7 cells compared with control EGFP-transfected cells (Fig. 6D to G), suggesting that Solo/Trio8 modulates early-to-late or early-to-recycling endosome transfer rather that endocytosis.

Solo/Trio8 localizes in axons and somatodendrites in primary cultured neurons. The gene for Solo/Trio8 is expressed in Purkinje neurons (Fig. 2B). Mature neurons have two polarized subcellular compartments, namely, axons and somatodendrites. Epithelial cells, including neurons, have polarized endosomes, that is, apical (axonal) endosomes and basolateral (somatodendrite) endosomes (2). To assess whether Solo/Trio8 localizes to early endosomes in a cell polarity-dependent manner in neuronal cells, we analyzed the EGFP-Solo distribution in primary cultured neurons. EGFP-Solo localized to small, Rab5-positive vesicles in soma (Fig. 7G to L), indicating localization to early endosomes. Moreover, EGFP-Solo was detected both in Map2-positive dendrites and in Tau1-positive axons (Fig. 7A to F). These results indicated that Solo localizes to both axons and somatodendrites in a cell polarity-independent manner.

Solo/Trio8 promotes neurite elongation in primary cultured neurons. Since endosomal membrane trafficking in neurons is involved in the regulation of neurite morphology (16, 19, 33), we analyzed the effects of Solo/Trio8 on neurite morphology in primary cultured cortical neurons. The total neurite length (axon and dendrite length) of the cortical neurons transfected with the EGFP-Solo expression construct significantly increased (about twofold) compared with cells transfected with the negative control EGFP construct (EGFP versus EGFP-Solo = 718.1 ± 66.8 μm versus 1,321.0 ± 111.4 μm; $n = 74$ and 97 neurons, respectively; $P < 0.01$; Fig. 8A and D). The EGFP-Solo expression construct also significantly increased (about twofold) the average maximal axon length in the primary cul-

incubated with Alexa 594-conjugated transferrin (25 μg/ml; D) or Sulforhodamine 101 (25 μg/ml; E) for 15 min and then fixed. Internalized transferrin or sulforhodamine (F and G) after 15 min of uptake was quantified by measuring the fluorescence intensity per cell as detected in panels D and E. The uptake of fluorescence for each construct is presented relative to that for EGFP-expressing cells (negative control; EGFP = 1.0). Each bar represents the mean ± the standard error of the mean (n = >10 cells for each construct). The differences in uptake between EGFP- and EGFP-Solo-expressing COS-7 cells were not significant (n.s.). Scale bars = 10 μm.

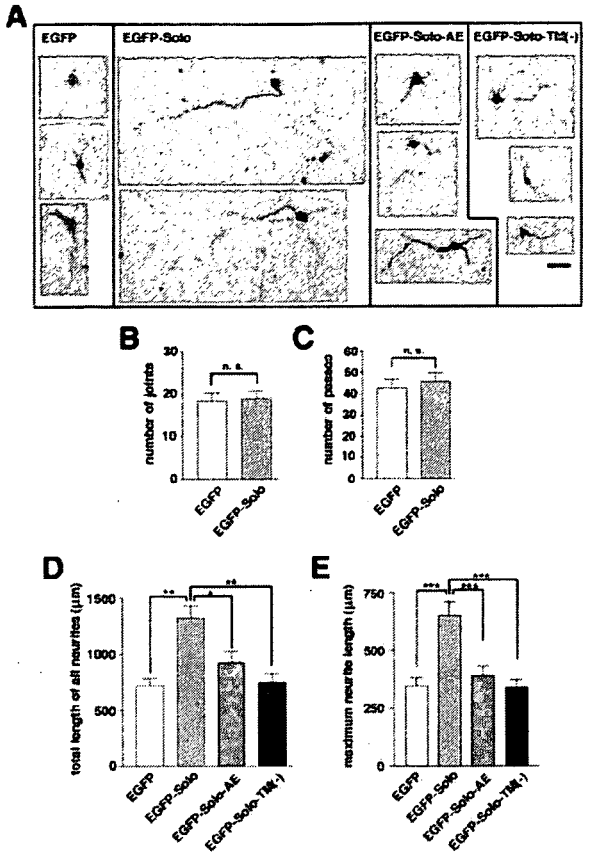

FIG. 8. Effects of Solo/Trio8 on neurite elongation in cultured cortical neurons. (A) Morphology of EGFP-Solo- or EGFP-Solo mutant-expressing neurons with anti-DsRed staining. Representative examples of fluorescence images (DsRed-derived signal; dark signals) of neurons transfected with control EGFP, EGFP-Solo, EGFP–Solo-AE, or EGFP–Solo-TM(−) constructs together with DsRed at 6 days in vitro are shown. To visualize the transfected neurons and their morphology, neurons were fixed and coimmunostained with anti-DsRed and anti-EGFP. Scale bar = 100 μm. (B and C) Quantification of the effects of EGFP and EGFP-Solo expression on the number of joints (branch points) (B) and passes (branch number) (C) per neuron (EGFP, n = 74; EGFP-Solo, n = 97). n.s., no significant difference. (D and E) Quantification of the effects of EGFP, EGFP-Solo, EGFP–Solo-AE, and EGFP–Solo-TM(−) expression on neurite length (total neurite length per neuron, dendrite length plus axon length) (D) and average maximal neurite length (axon length per neuron) (E) [EGFP, n = 74; EGFP-Solo, n = 97; EGFP–Solo-AE, n = 60; EGFP–Solo-TM(−), n = 91]. Each bar represents the mean ± the standard error of the mean. *, $P < 0.05$; **, $P < 0.01$; ***, $P < 0.001$.

tured neurons (EGFP versus EGFP-Solo = 347.3 ± 35.64 μm versus 650.9 ± 60.94 μm; n = 74 and 97 neurons, respectively; $P < 0.001$; Fig. 8E). Mutant Solo expression constructs EGFP–Solo-AE and EGFP–Solo-TM(−) failed to induce either total neurite length or maximal elongation (Fig. 8A, D, and E). The number of joints (branch points) and passes (branches) did not change significantly upon EGFP-Solo expression (Fig. 8B and C). We were unable to quantify the total number of early endosomes per neuron because the size and complexity of neurons relative to COS-7 cells (Fig. 6) precluded the detection of all early endosomes with sufficient resolution in a single image. However, EGFP-Solo was distributed in a vesicle-like pattern (similar to that in COS-7 cells) in axons and dendrites of neurons (Fig. 7 and data not shown), and this pattern was altered upon expression of Solo-AE or Solo-TM(−) (data not shown), as observed in COS-7 cells (Fig. 6A).

Solo/Trio8 siRNA affects calbindin D28k-positive neurite length in the granule cell layer of the cerebellum. We attempted to knock down expression of the gene for Solo/Trio8 by RNA interference. To find an RNA sequence that would be effective, we prepared seven siRNAs with different Solo/Trio8-specific target recognition sequences that lacked homology to other sequences in the mouse genome. We then transfected each siRNA together with the EGFP-Solo expression construct into COS-7 cells. Transfection of the siRNA (region, bp 5483 to 5505) with a target sequence in the potential membrane-anchoring domain of Solo significantly reduced the level of Solo protein by ~25% (Fig. 9B and C) compared with that of COS-7 cells transfected with negative control scrambled siRNA no. 1 (Fig. 9A and C), negative control siRNA no. 2 (purchased from Ambion), or no siRNA (data not shown). The Solo/Trio8-specific siRNA did not affect the level of EGFP in cells transfected with the EGFP expression construct compared with negative control siRNA (data not shown). To investigate the role of Solo/Trio8 in neurite morphology, we transfected the Solo/Trio8-specific siRNA or negative control scrambled siRNAs into cells of organotypic brain slices (44) by a liposome-based in vivo siRNA-transfer method (51) that we had previously established. We prepared coronally sliced P11 cerebellar slices and cut them into left and right halves (Fig. 9D). One of the halves was transfected with Solo/Trio8-specific siRNA, and the other half was transfected with negative control siRNA. We confirmed efficient incorporation of transfected Cy3-labeled control siRNA no. 1 into cells in the cerebellar slice by confocal laser scanning microscopy (data not shown). We fixed the slices 2 days after transfection and stained them with anti-calbindin D28k to specifically visualize the morphology of Purkinje neurons. The lengths of calbindin D28k-positive neurites (axons of Purkinje neurons) in the granule cell layer of slices transfected with Solo/Trio8 siRNA were significantly shorter (39.2%; n = 4; P = 0.0039, Student's t test) than those of slices transfected with negative control siRNA no. 1 (Fig. 9E to I), suggesting that Solo/Trio8 is essential for neurite elongation or maintenance of Purkinje axon length. The neurite morphology of neurons transfected with negative control siRNA no. 1, siRNA no. 2, or EGFP siRNA (purchased from Ambion) was not changed compared with that of untransfected Purkinje neurons (data not shown).

DISCUSSION

A number of early-endosome-specific proteins have been identified to date. Among them, EEA1, a specific effector of Rab5, binds to early-endosomal membranes (5, 45). This localization of EEA1 is mediated via its FYVE domain that interacts with phosphatidylinositol 3-phosphate, whose intracellular distribution is restricted primarily to early endosomes (21). In the present study, DNA microarray analysis of pcd mice led us to identify a mouse Trio splice variant, Solo/Trio8, which localizes to early endosomes. Although Solo/Trio8 is likely embedded in the endosomal membrane (Fig. 3, 4, 6, and

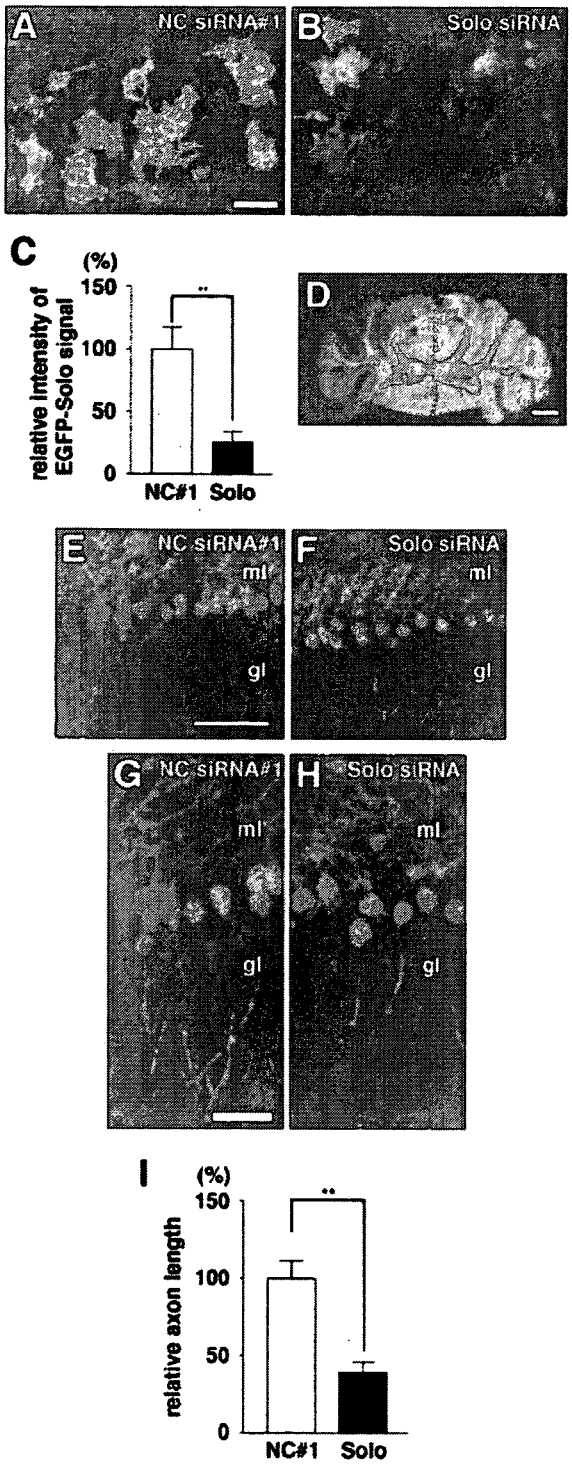

FIG. 9. Effects of Solo/Trio8 siRNA on Purkinje neurons. COS-7 cells were cotransfected with vectors encoding either EGFP-Solo and control scrambled siRNA (A, negative control [NC] siRNA no. 1) or EGFP-Solo and Solo/Trio8 siRNA (B, Solo siRNA) and then stained with anti-GFP (green) and DAPI (blue). (C) Effect of siRNA on EGFP-Solo expression quantified by measuring the fluorescence intensity per cell as detected in panels A and B. The effect of Solo siRNA on EGFP-Solo suppression is presented relative to that of negative control siRNA no. 1 (100%). Each bar represents the mean ± the standard error of the mean (n = >10 cells). Significant differences are indicated by double asterisks ($P < 0.01$; t test). Scale bar = 50 μm. (D) Overview of a coronally sliced cerebellum. Scale bar = 1 mm. Cerebellar slices derived from P11 were cut into left and right halves (at the red dotted line). One of the halves was transfected with Solo/Trio8-specific siRNA (F and H; Solo siRNA), and the another half was transfected with negative control siRNA no. 1 (E and G) at 1 day in vitro and then cultured for 2 days. Slices were stained with anti-calbindin D28k (green), showing the morphology of Purkinje cells. Panels G and H are high-magnification images of panels E and F, respectively. gl, granule cell layer; ml, molecular cell layer. The scale bar in panel E is 100 μm (E and F), and that in panel G is 50 μm (G and H). (I) Quantitative representation of the effect of Solo/Trio8 siRNA on the axon length of Purkinje neurons in the granule cell layer. The relative axon length for Solo siRNA is presented relative to that for negative control siRNA no. 1 (100%). Each bar represents the mean ± the standard error of the mean (n = 4 slices). Significant differences are indicated by double asterisks ($P < 0.01$; t test).

7), it does not contain a canonical FYVE-like motif. It is not clear which domain actively recruits Solo/Trio8 to early endosomes; however, an N-terminal region may be required for the recruitment since this region contains a sec14-like domain and spectrin-like repeats. Yeast Sec14 is a phosphatidylinositol transfer protein that catalyzes the exchange of phosphatidylinositol for phosphatidylcholine in membranes (43), suggesting that the sec14-like domain of Solo/Trio8 may function to link it to phosphatidylinositol 3-phosphate in early endosomes. The spectrin-like repeats constitute interaction sites for cytoskeletal and signal transduction proteins (8) and may facilitate the association of Solo/Trio8 (directly or indirectly) with early-endosome membranes. Cooperative interactions between the N- and C-terminal domains are likely to be important for targeting Solo to the early endosome and thus may represent a novel mechanism for protein localization to this organelle.

Solo/Trio8 mRNA expression was restricted to Purkinje neurons in the cerebellum and markedly increased during the maturation stage of these neurons after birth (Fig. 5A). EEA1-positive early-endosome signals also markedly increased in Purkinje neurons during this stage (Fig. 5B). We demonstrated that overexpression of Solo/Trio8 augmented the number of EEA1-positive early-endosomal vesicles in COS-7 cells, and the abrogation of Solo GEF1 activity attenuated this increase and disrupted the cellular distribution of early endosomes (Fig. 6). Taken together, these results suggest that Solo/Trio8 promotes postnatal maturation of the early-endosome pool in Purkinje neurons. Our data also suggest that Solo/Trio8 GEF1 activity is essential for the localization of this protein to early endosomes, and it may affect the maturation of the early-endosome pool directly via some small GTPases. The Trio GEF1 domain activates both Rac1 (Fig. 3B) and RhoG (3), and therefore Solo/Trio8 GEF1 may also activate downstream early-endosomal Rac1- or RhoG-type small GTPases. More than 150 small GTPases have been identified in the human genome, and the Rac1- and RhoG-type subfamily includes Rac1 to -3, RhoG, CDC42h, CDC42, TC10, and TCL (15). Among these, Rac1 and TC10 are present in endosomes (26, 27) but it is not known if either protein is a direct target for Solo/Trio8 GEF1 in early endosomes. Solo/Trio8 may activate multiple Rac1/RhoG-type small GTPases, each of which may

have a discrete function in early endosomes. Cellular Rac1 (26) had a distribution pattern distinct from that of Solo/Trio8, and Rac1 activation (Fig. 3) did not correlate with the increase in early endosomes induced by WT or mutant Solo/Trio8 (Fig. 6). Thus, Rac1 is unlikely to be the direct downstream target of Solo/Trio8. Identification of in vivo downstream targets for Solo/Trio8 may enhance our understanding of how Rho family GTPases regulate endosomal vesicle trafficking.

EGFP-Solo proteins were distributed in Tau1-positive axons, Map2-positive dendrites were distributed in cortical neurons (Fig. 7), and transfection of the EGFP-Solo construct induced both dendrite and axon elongation in these neurons (Fig. 8). These data indicate that Solo/Trio8 functions in a cell polarity-independent manner to regulate neuronal morphology. Furthermore, GEF1 activity and the C-terminal membrane-anchoring domain of Solo/Trio8 were essential for induction of not only neurite elongation but also of an increase in the number of early endosomes (Fig. 6 and 8). These equivalent domain requirements indicate that both biological activities are exhibited upon activation of early-endosome-associated Rho family GTPases, suggesting that Solo/Trio8 functions as an early-endosome-associated GEF to control cell polarity-independent neurite morphogenesis.

To date, two Trio family members, Trio and Kalirin, have been identified in mammals (3). The domain structure of Kalirin is nearly identical to that of Trio, and its expression is specific to the central nervous system (3). In addition, several short isoforms of Kalirin have been identified (18). Full-length Kalirin localizes to neuronal soma, where it displays a cytoplasmic protein-like diffuse immunostaining pattern. Interestingly, a Kalirin splice variant, Duo/Kalirin-7, lacking the C-terminal GEF2 and kinase domains (that is, a structure similar to that of Solo/Trio8) localizes to small punctate structures at neuronal processes and dendritic spines (18, 38). Duo/Kalirin-7 is involved in signal transduction during dendritic spine morphogenesis mediated by activation of the ephrinB receptor (37). We thus postulate that some of the cell surface receptors or adhesion molecules controlling neurite morphology are involved in Solo/Trio8-induced neurite elongation via the regulation of early-endosome dynamics.

Upstream effectors of endosome-specific Rab family small GTPases that localize to early endosomes have previously been characterized (39, 46). However, the activation mechanism of Rho family small GTPases that function in early endosomes is not well understood. Here, we identified Solo/Trio8 as a candidate upstream effector of Rho family GTPases that localize to early endosomes. The subcellular localization of Solo/Trio8 is mediated through a C-terminal membrane-anchoring domain and its GEF1 activity (Fig. 6A, EGFP–Solo-AE), and it is plausible that its endosomal localization may directly activate Rac1/RhoG-type small GTPases that sequentially modulate the dynamics of early endosomes. Our results show that Solo/Trio8 gene expression significantly increases during the postnatal maturation stage of Purkinje neurons in the cerebellum (Fig. 5). We also demonstrate that a Solo/Trio8-specific siRNA induces loss of calbindin D28k-positive neurite morphology in cultured cerebellar slices (Fig. 9). These data suggest that changes in early-endosome dynamics, as modulated by Solo, control neurite morphogenesis and/or maintenance of Purkinje neurons in vivo.

ACKNOWLEDGMENTS

This work was supported by Grants-in-Aid for Scientific Research from the Ministry of Health, Labor and Welfare of Japan; Grants-in-Aid for Scientific Research from the Ministry of Education, Culture, Sports, Science and Technology of Japan; a grant from Pharmaceuticals and Medical Devices Agency; and a grant from the Japan Science and Technology Agency.

REFERENCES

1. **Aoki, S., Q. Su, H. Li, K. Nishikawa, K. Ayukawa, Y. Hara, K. Namikawa, S. Kiryu-Seo, H. Kiyama, and K. Wada.** 2002. Identification of an axotomy-induced glycosylated protein, AIGP1, possibly involved in cell death triggered by endoplasmic reticulum-Golgi stress. J. Neurosci. **22**:10751–10760.
2. **Apodaca, G.** 2001. Endocytic traffic in polarized epithelial cells: role of the actin and microtubule cytoskeleton. Traffic **2**:149–159.
3. **Bateman, J., and D. Van Vactor.** 2001. The Trio family of guanine-nucleotide-exchange factors: regulators of axon guidance. J. Cell Sci. **114**:1973–1980.
4. **Benard, V., and G. M. Bokoch.** 2002. Assay of Cdc42, Rac, and Rho GTPase activation by affinity methods. Methods Enzymol. **345**:349–359.
5. **Christoforidis, S., H. M. McBride, R. D. Burgoyne, and M. Zerial.** 1999. The Rab5 effector EEA1 is a core component of endosome docking. Nature **397**:621–625.
6. **Debant, A., C. Serra-Pages, K. Seipel, S. O'Brien, M. Tang, S. H. Park, and M. Streuli.** 1996. The multidomain protein Trio binds the LAR transmembrane tyrosine phosphatase, contains a protein kinase domain, and has separate rac-specific and rho-specific guanine nucleotide exchange factor domains. Proc. Natl. Acad. Sci. USA **93**:5466–5471.
7. **Delcroix, J. D., J. S. Valletta, C. Wu, S. J. Hunt, A. S. Kowal, and W. C. Mobley.** 2003. NGF signaling in sensory neurons: evidence that early endosomes carry NGF retrograde signals. Neuron **39**:69–84.
8. **Djinovic-Carugo, K., M. Gautel, J. Ylanne, and P. Young.** 2002. The spectrin repeat: a structural platform for cytoskeletal protein assemblies. FEBS Lett. **513**:119–123.
9. **Dumas, J. J., E. Merithew, E. Sudharshan, D. Rajamani, S. Hayes, D. Lawe, S. Corvera, and D. G. Lambright.** 2001. Multivalent endosome targeting by homodimeric EEA1. Mol. Cell **8**:947–958.
10. **Estrach, S., S. Schmidt, S. Diriong, A. Penna, A. Blangy, P. Fort, and A. Debant.** 2002. The human Rho-GEF trio and its target GTPase RhoG are involved in the NGF pathway, leading to neurite outgrowth. Curr. Biol. **12**:307–312.
11. **Feng, Y., B. Press, and A. Wandinger-Ness.** 1995. Rab 7: an important regulator of late endocytic membrane traffic. J. Cell Biol. **131**:1435–1452.
12. **Fernandez-Gonzalez, A., A. R. La Spada, J. Treadaway, J. C. Higdon, B. S. Harris, R. L. Sidman, J. I. Morgan, and J. Zuo.** 2002. Purkinje cell degeneration (pcd) phenotypes caused by mutations in the axotomy-induced gene, Nna1. Science **295**:1904–1906.
13. **Gasman, S., Y. Kalaidzidis, and M. Zerial.** 2003. RhoD regulates endosome dynamics through Diaphanous-related Formin and Src tyrosine kinase. Nat. Cell Biol. **5**:195–204.
14. **Gomez, G. A., and J. L. Daniotti.** 2005. H-Ras dynamically interacts with recycling endosomes in CHO-K1 cells: involvement of Rab5 and Rab11 in the trafficking of H-Ras to this pericentriolar endocytic compartment. J. Biol. Chem. **280**:34997–35010.
15. **Heo, W. D., and T. Meyer.** 2003. Switch-of-function mutants based on morphology classification of Ras superfamily small GTPases. Cell **113**:315–328.
16. **Huang, E. J., H. Li, A. A. Tang, A. K. Wiggins, R. L. Neve, W. Zhong, L. Y. Jan, and Y. N. Jan.** 2005. Targeted deletion of numb and numblike in sensory neurons reveals their essential functions in axon arborization. Genes Dev. **19**:138–151.
17. **Jarousse, N., and R. B. Kelly.** 2001. Endocytotic mechanisms in synapses. Curr. Opin. Cell Biol. **13**:461–469.
18. **Johnson, R. C., P. Penzes, B. A. Eipper, and R. E. Mains.** 2000. Isoforms of kalirin, a neuronal Dbl family member, generated through use of different 5′- and 3′-ends along with an internal translational initiation site. J. Biol. Chem. **275**:19324–19333.
19. **Kimura, K., A. Mizoguchi, and C. Ide.** 2003. Regulation of growth cone extension by SNARE proteins. J. Histochem. Cytochem. **51**:429–433.
20. **Kroschewski, R., A. Hall, and I. Mellman.** 1999. Cdc42 controls secretory and endocytic transport to the basolateral plasma membrane of MDCK cells. Nat. Cell Biol. **1**:8–13.
21. **Kutateladze, T., and M. Overduin.** 2001. Structural mechanism of endosome docking by the FYVE domain. Science **291**:1793–1796.
22. **Linnik, K. M., and H. Herscovitz.** 1998. Multiple molecular chaperones interact with apolipoprotein B during its maturation. The network of endoplasmic reticulum-resident chaperones (ERp72, GRP94, calreticulin, and BiP) interacts with apolipoprotein b regardless of its lipidation state. J. Biol. Chem. **273**:21368–21373.
23. **Liu, X., H. Wang, M. Eberstadt, A. Schnuchel, E. T. Olejniczak, R. P. Meadows, J. M. Schkeryantz, D. A. Janowick, J. E. Harlan, E. A. Harris, D. E. Staunton, and S. W. Fesik.** 1998. NMR structure and mutagenesis of

the N-terminal Dbl homology domain of the nucleotide exchange factor Trio. Cell **95**:269–277.
24. **Maeda, N., M. Niinobe, and K. Mikoshiba.** 1990. A cerebellar Purkinje cell marker P400 protein is an inositol 1,4,5-trisphosphate (InsP3) receptor protein. Purification and characterization of InsP3 receptor complex. EMBO J. **9**:61–67.
25. **McPherson, C. E., B. A. Eipper, and R. E. Mains.** 2005. Multiple novel isoforms of Trio are expressed in the developing rat brain. Gene **347**:125–135.
26. **Michaelson, D., J. Silletti, G. Murphy, P. D'Eustachio, M. Rush, and M. R. Philips.** 2001. Differential localization of Rho GTPases in live cells: regulation by hypervariable regions and RhoGDI binding. J. Cell Biol. **152**:111–126.
27. **Miura, K., S. Miyazawa, S. Furuta, J. Mitsushita, K. Kamijo, H. Ishida, T. Miki, K. Suzukawa, J. Resau, T. D. Copeland, and T. Kamata.** 2001. The Sos1-Rac1 signaling. Possible involvement of a vacuolar H^+-ATPase E subunit. J. Biol. Chem. **276**:46276–46283.
28. **Mohrmann, K., and P. van der Sluijs.** 1999. Regulation of membrane transport through the endocytic pathway by rabGTPases. Mol. Membr. Biol. **16**:81–87.
29. **Mukherjee, S., R. N. Ghosh, and F. R. Maxfield.** 1997. Endocytosis. Physiol. Rev. **77**:759–803.
30. **Mullen, R. J., E. M. Eicher, and R. L. Sidman.** 1976. Purkinje cell degeneration, a new neurological mutation in the mouse. Proc. Natl. Acad. Sci. USA **73**:208–212.
31. **Munro, S., and H. R. Pelham.** 1986. An Hsp70-like protein in the ER: identity with the 78 kd glucose-regulated protein and immunoglobulin heavy chain binding protein. Cell **46**:291–300.
32. **Nielsen, E., F. Severin, J. M. Backer, A. A. Hyman, and M. Zerial.** 1999. Rab5 regulates motility of early endosomes on microtubules. Nat. Cell Biol. **1**:376–382.
33. **Nishimura, T., Y. Fukata, K. Kato, T. Yamaguchi, Y. Matsuura, H. Kamiguchi, and K. Kaibuchi.** 2003. CRMP-2 regulates polarized Numb-mediated endocytosis for axon growth. Nat. Cell Biol. **5**:819–826.
34. **Nordquist, D. T., C. A. Kozak, and H. T. Orr.** 1988. cDNA cloning and characterization of three genes uniquely expressed in cerebellum by Purkinje neurons. J. Neurosci. **8**:4780–4789.
35. **O'Brien, S. P., K. Seipel, Q. G. Medley, R. Bronson, R. Segal, and M. Streuli.** 2000. Skeletal muscle deformity and neuronal disorder in Trio exchange factor-deficient mouse embryos. Proc. Natl. Acad. Sci. USA **97**:12074–12078.
36. **Otomo, A., S. Hadano, T. Okada, H. Mizumura, R. Kunita, H. Nishijima, J. Showguchi-Miyata, Y. Yanagisawa, E. Kohiki, E. Suga, M. Yasuda, H. Osuga, T. Nishimoto, S. Narumiya, and J. E. Ikeda.** 2003. ALS2, a novel guanine nucleotide exchange factor for the small GTPase Rab5, is implicated in endosomal dynamics. Hum. Mol. Genet. **12**:1671–1687.
37. **Penzes, P., A. Beeser, J. Chernoff, M. R. Schiller, B. A. Eipper, R. E. Mains, and R. L. Huganir.** 2003. Rapid induction of dendritic spine morphogenesis by trans-synaptic ephrinB-EphB receptor activation of the Rho-GEF kalirin. Neuron **37**:263–274.
38. **Penzes, P., R. C. Johnson, R. Sattler, X. Zhang, R. L. Huganir, V. Kambampati, R. E. Mains, and B. A. Eipper.** 2001. The neuronal Rho-GEF Kalirin-7 interacts with PDZ domain-containing proteins and regulates dendritic morphogenesis. Neuron **29**:229–242.
39. **Pfeffer, S.** 2003. Membrane domains in the secretory and endocytic pathways. Cell **112**:507–517.
40. **Ren, M., G. Xu, J. Zeng, C. De Lemos-Chiarandini, M. Adesnik, and D. D. Sabatini.** 1998. Hydrolysis of GTP on rab11 is required for the direct delivery of transferrin from the pericentriolar recycling compartment to the cell surface but not from sorting endosomes. Proc. Natl. Acad. Sci. USA **95**: 6187–6192.
41. **Rico, B., H. E. Beggs, D. Schahin-Reed, N. Kimes, A. Schmidt, and L. F. Reichardt.** 2004. Control of axonal branching and synapse formation by focal adhesion kinase. Nat. Neurosci. **7**:1059–1069.
42. **Schmidt, A., and A. Hall.** 2002. Guanine nucleotide exchange factors for Rho GTPases: turning on the switch. Genes Dev. **16**:1587–1609.
43. **Sha, B., S. E. Phillips, V. A. Bankaitis, and M. Luo.** 1998. Crystal structure of the Saccharomyces cerevisiae phosphatidylinositol-transfer protein. Nature **391**:506–510.
44. **Shima, Y., M. Kengaku, T. Hirano, M. Takeichi, and T. Uemura.** 2004. Regulation of dendritic maintenance and growth by a mammalian 7-pass transmembrane cadherin. Dev. Cell **7**:205–216.
45. **Simonsen, A., R. Lippe, S. Christoforidis, J. M. Gaullier, A. Brech, J. Callaghan, B. H. Toh, C. Murphy, M. Zerial, and H. Stenmark.** 1998. EEA1 links PI(3)K function to Rab5 regulation of endosome fusion. Nature **394**: 494–498.
46. **Somsel Rodman, J., and A. Wandinger-Ness.** 2000. Rab GTPases coordinate endocytosis. J. Cell Sci. **113**(Pt. 2):183–192.
47. **Symons, M., and N. Rusk.** 2003. Control of vesicular trafficking by rho GTPases. Curr. Biol. **13**:R409–R418.
48. **Tanaka, M., N. Maeda, M. Noda, and T. Marunouchi.** 2003. A chondroitin sulfate proteoglycan PTPζ/RPTPβ regulates the morphogenesis of Purkinje cell dendrites in the developing cerebellum. J. Neurosci. **23**:2804–2814.
49. **Tanaka, M., A. Tomita, S. Yoshida, M. Yano, and H. Shimizu.** 1994. Observation of the highly organized development of granule cells in rat cerebellar organotypic cultures. Brain Res. **641**:319–327.
50. **van der Luit, A. H., M. Budde, P. Ruurs, M. Verheij, and W. J. van Blitterswijk.** 2002. Alkyl-lysophospholipid accumulates in lipid rafts and induces apoptosis via raft-dependent endocytosis and inhibition of phosphatidylcholine synthesis. J. Biol. Chem. **277**:39541–39547.
51. **Wang, Y. L., W. Liu, E. Wada, M. Murata, K. Wada, and I. Kanazawa.** 2005. Clinico-pathological rescue of a model mouse of Huntington's disease by siRNA. Neurosci. Res. **53**:241–249.

GLIA 55:317–327 (2007)

PACAP/PAC1 Autocrine System Promotes Proliferation and Astrogenesis in Neural Progenitor Cells

MIKA NISHIMOTO,[1,2] AKIKO FURUTA,[1] SHUNSUKE AOKI,[1,3,4] YOSHIHISA KUDO,[2] HIROYOSHI MIYAKAWA,[2] AND KEIJI WADA[1,4*]

[1]*Department of Degenerative Neurological Diseases, National Institute of Neuroscience, National Center of Neurology and Psychiatry, Kodaira, Tokyo, Japan*

[2]*Laboratory of Cellular Neurobiology, Tokyo University of Pharmacology and Life science, Hachioji, Tokyo, Japan*

[3]*NEDO (New Energy and Industrial Technology Development Organization), Kawasaki, Kanagawa, Japan*

[4]*Core Research for Evolutional Science and Technology (CREST), Japan Science and Technology Agency (JST), Kawaguchi, Saitama, Japan*

KEY WORDS

pituitary adenylate cyclase-activating polypeptide (PACAP); PAC1; neural progenitor cell; autocrine proliferation factor

ABSTRACT

The Pituitary adenylate cyclase-activating peptide (PACAP) ligand/type 1 receptor (PAC1) system regulates neurogenesis and gliogenesis. It has been well established that the PACAP/PAC1 system induces differentiation of neural progenitor cells (NPCs) through the Gs-mediated cAMP-dependent signaling pathway. However, it is unknown whether this ligand/receptor system has a function in proliferation of NPCs. In this study, we identified that PACAP and PAC1 were highly expressed and co-localized in NPCs of mouse cortex at embryonic day 14.5 (E14.5) and found that the PACAP/PAC1 system potentiated growth factor-induced proliferation of mouse cortical NPCs at E14.5 via Gq-, but not Gs-, mediated PLC/IP_3-dependent signaling pathway in an autocrine manner. Moreover, PAC1 activation induced elongation of cellular processes and a stellate morphology in astrocytes that had the bromodeoxyuridine (BrdU)-incorporating ability of NPCs. Consistent with this notion, we determined that the most BrdU positive NPCs differentiated to astrocytes through PAC1 signaling. These results suggest that the PACAP/PAC1 system may play a dual role in neural/glial progenitor cells not only differentiation but also proliferation in the cortical astrocyte lineage via Ca^{2+}-dependent signaling pathways through PAC1.

INTRODUCTION

Multipotent and proliferative neural progenitor cells (NPCs) represent the epigenetic and intrinsic origin of neurons, astrocytes, and oligodendrocytes in the central nervous system (CNS) (Altman and Bayer, 1990a,b; Reynolds et al., 1992; Reynolds and Weiss, 1996). During brain development, neurogenesis and gliogenesis occur as distinct temporal events with only some overlap. In the mouse embryonic cortex, neurogenesis takes place between embryonic days (E) 12 and 17 to generate neurons from neuronal progenitors. In contrast, astrocytic differentiation begins mainly at E16 and continues in the postnatal days. In each embryonic stage, NPC proliferation or differentiation is mostly regulated by locally produced or peripherally circulating soluble paracrine factors such as growth factors (e.g. basic fibroblast growth factor (b-FGF) and epidermal growth factor (EGF)) and cytokines as well as several autocrine factors such as bone morphogenic protein-4 (BMP4), interleukin 6, glycosylated cystatin C, and insulin-like growth factors (Eccleston et al., 1991; Liu et al., 2004; Wislet-Gendebien et al., 2004). Although glial progenitors are known to arise from NPCs predominantly at a delay on neurogenesis, the underlying spatiotemporal regulatory mechanisms of proliferation and differentiation of glial progenitors are not yet defined.

The effects of pituitary adenylate cyclase-activating peptide (PACAP) and vasoactive intestinal peptide (VIP), which are members of the VIP/secretin/glucagon peptide family have been well characterized in the CNS. For example, these factors affect neurotransmitter release and survival of hippocampal neurons as well as controlling cerebellar maturation (Arimura, 1998; Basille et al., 1993; Bluet-Pajot et al., 1998; Otto et al., 2001; Rayan et al., 1991; Vaudry et al., 2002; Zhou et al., 2002). These PACAP and VIP functions are mediated by three PACAP receptors, PAC1, VPAC1, and VPAC2 (Christophe, 1993; Muller et al., 1995; Tatsuno et al., 1994; Zhou et al., 2002). In particular, PACAP and PAC1 are highly expressed and distributed ubiquitously in the embryonic CNS and peripheral nervous system (Tatsuno et al., 1994; Zhou et al., 2002). Accordingly, PACAP is considered to influence the regulation of NPC proliferation and/or differentiation during embryonic development (Dicicco-Bloom et al., 1998). The PAC1 gene encodes a

Grant sponsors: Grants-in Aid for Scientific Research, Japanese Society for Promotion of Science; Research Grant in Priority Area Research, Ministry of Education, Culture, Sports, Science and Technology, Japan; Grants-in-Aid for Scientific Research, Ministry of Health, Labour and Welfare, Japan; CREST, Japanese Science and Technology Agency; Program for Promotion of Fundamental Studies, National Institute of Biomedical Innovation (NIBIO).

*Correspondence to: Keiji Wada, Department of Degenerative Neurological Diseases, National Institute of Neuroscience, National Center of Neurology and Psychiatry (NCNP), Kodaira 4-1-1, Tokyo 187-8502, Japan. E-mail: wada@ncnp.go.jp

Received 22 June 2006; Revised 18 October 2006; Accepted 20 October 2006

DOI 10.1002/glia.20461

Published online 17 November 2006 in Wiley InterScience (www.interscience.wiley.com).

G-protein-coupled receptor that has four splice variants, depending on the presence or absence of either one or two of the cassettes, "hip" and "hop," in the third intercellular loop (Bresson-Bepoldin et al., 1998; Jaworski and Proctor, 2000; Zhou et al., 2000a,b). These splice variants are involved in multiple and response-specific second messenger cascades (Pisegna et al., 1996). Evidence from studies with transfected cells indicates that each splice variant activates different cell signaling pathways involving adenylate cyclase (AC) and/or phospholipase C (PLC) and activation of these two pathways has opposite effects on the proliferation of cerebral cortical precursor cells (Basille et al., 1995; Cazillis et al., 2004; Lu et al., 1998; Mercer et al., 2004; Suh et al., 2001; Waschek et al., 2000). Recently it was shown that the PACAP/PAC1 system inhibits NPC proliferation and promotes neurogenesis and gliogenesis by activation of the Gs-mediated cAMP-dependent signal transduction pathway in the embryonic brain (Lelievre et al., 2002; Suh et al., 2001; Waschek et al., 1998). In contrast, PACAP was reported to promote adult NPC proliferation via PAC1 both in vivo and in vitro. Thus the precise effect of direct activation of PAC1 signaling on embryonic NPCs, and the mechanism thereof, remains unknown.

To elucidate the function of PACAP in embryonic cortical NPCs, we investigated regulatory mechanisms of PAC1 signaling for cell proliferation and differentiation using NPCs of mouse cortex at E14.5 when cortical NPCs in the ventricular zone (VZ)/subventricular zone (SVZ) contain not only neuronal progenitors but also glial progenitors. In this study, we identified that PACAP and PAC1 were highly expressed and co-localized in NPCs. Surprisingly, we found that the PACAP/PAC1 system potentiated growth factor-induced proliferation in mouse cortical NPCs at E14.5 via Gq-mediated—but not Gs-mediated—PLC/IP_3-dependent signaling pathways in an autocrine manner. Moreover, we showed that direct activation of PAC1 induced astrocyte-like morphological changes in embryonic cortical NPCs. Together with our present results and the previously identified role of PACAP, we suggest a dual role of the PACAP/PAC1 system for NPC proliferation during cortical astrogenesis by different signaling pathways of PAC1 variants at E14.5.

MATERIALS AND METHODS

Antibodies and Reagents

Monoclonal and polyclonal antibodies used in this study were as follows: mouse monoclonal anti-nestin (Becton Dickinson, Lexington, KY, and RaZ 401; Developmental Studies Hybridema Bank, Iowa City, IA), mouse monoclonal anti-neuronal class III β-tubulin (anti-β III tubulin (Tuj1); COVANCE, Berkeley, CA), mouse monoclonal anti-galactocerebroside (anti-Gal C; Chemicon International, Temecula, CA), rabbit polyclonal anti-glial fibrillary acidic protein (anti-GFAP: DAKO, Carpinteria, CA), goat polyclonal anti-PAC1 (gift from A. Arimura, Tulane University, New Orleans), rabbit polyclonal anti-PACAP38 (Calbiochem, San Diego, CA), rat monoclonal anti-bromodeoxyuridine (BrdU; Becton Dickinson, Lexington, KY). The secondary antibodies conjugated to Alexa Fluor fluorescein (goat anti-mouse Alexa Fluor 488, 568, or 633, goat anti-rabbit Alexa Fluor 488 or 568, rabbit anti-goat Alexa Fluor 594, and goat anti-mouse Alexa Fluor 488 or 568) were purchased from Molecular Probes (Eugene, OR). PACAP38, PACAP(6–38) (Peptide Institute, Osaka, Japan), VIP (Sigma, St. Louis, MO), maxadilan and M65 (gifts from Dr. Richard G. Titus, Colorado State University) were dissolved in distilled water. H89, 2-aminoethoxydiphenyl borate (2-APB; Calbiochem, San Diego, CA), chelerythrine (Sigma) and *O,O′*-bis(2-aminophenyl)ethyleneglycol-*N,N,N′,N′*-tetraacetic acid (BAPTA-AM; Sigma) were dissolved in DMSO. Each solution was added to the medium, and the final concentration of organic solvent (DMSO) in the medium was adjusted to no more than 0.1% (v/v). Each control medium contained the same amount of each organic solvent.

Animals

Pregnant C57BL/6J mice were purchased from CLEA Japan. All experiments were performed in the laboratory for animal experiments according to NIH Standards for Treatment of Laboratory Animals.

Culture of Mouse Embryonic Cortical NPCs

Cortical NPCs were cultured as previously described (Li et al., 2001; Nakashima et al., 1999). Briefly, embryos were removed from pregnant C57BL/6J mice (CLEA Japan, Tokyo, Japan) and staged according to morphological criteria to confirm gestational day (Kaufman, 1998). Developing mouse cerebral cortices were dissected at embryonic day 14.5 (E14.5). Cells were mechanically dissociated by trituration and plated at a density of 3.0×10^6 cells in 10-cm dishes (BD) that were precoated with 15 μg/mL poly-×L-ornithine (Sigma) and 1 μg/mL fibronectin (Nitta Gelatin, Osaka, Japan). Cells were expanded for 4 days in serum-free Neurobasal (NB) medium (Invitrogen, Carlsbad, CA) supplemented with B27 (Invitrogen), 0.5 mM L-glutamine (Invitrogen), 100 μg/mL penicillin and 100 μg/mL streptomycin (Invitrogen). This medium was supplemented with 10 ng/mL b-FGF (PeproTech, Rocky Hill, NJ), except where indicated otherwise. Cultures were maintained at 37°C in an atmosphere of 95% air and 5% CO_2. For secondary culture, b-FGF-expanded cortical NPCs were washed in warm Hanks' balanced salt solution, detached via mechanically pipetting, and resuspended in NB medium. Cells were then reseeded in 24-well plates (Nunc; 1×10^5 cells per well), 48-well plates (Nunc; 4.5×10^4 cells/well) or 96-well plates (Nunc; 1×10^4 cells/well) precoated with poly-L-ornithine and fibronectin.

Conditioned Medium Preparation

Subconfluent embryonic cortical NPCs in secondary cultures and control cultures maintained without

NvvPCs were incubated in serum-free NB/B27 medium for 48 h with b-FGF (5 ng/mL). After this period, conditioned medium derived from either NPCs or control cultures was collected and centrifuged at 1,000*g* for 5 min at 4°C to remove nonadherent cells.

Real-Time RT-PCR

Total RNA was isolated from cultured embryonic cortical NPCs and E14 mouse cerebral cortex. These RNAs (1 μg) were treated with DNase I and converted to cDNA using Superscript reverse transcriptase (Invitrogen) and random hexamer primers, according to the manufacturer's instructions. Real-time quantitative RT-PCR was performed with the SYBR Green-based method (ABI PRISM 7700 Sequence Detection System, Perkin-Elmer). The quantitative RT-PCR method (User Bulletin no. 2, Applied Biosystems, Foster City, CA) was modified to establish an expression level index for mRNA, and the SYBR green signal for the hypoxanthine-guanine phosphoribosyl transferase (hprt) gene amplicon was used as a reference. Amplification efficiency was determined and confirmed in a control PCR experiment using serially diluted cDNAs as templates. Real-time RT-PCR reactions were run on an ABI PRISM 7700 Sequence Detection System device using the following program: 2 min at 50°C, 10 min at 95°C and 40 cycles of 15 s at 95°C and 1 min at 60°C. The real-time RT-PCR products were analyzed using the sequence detection system software 1.7 (Applied Biosystems). The analysis and calculations were performed as described above. The efficiency of reverse transcription and the quality of cDNA was assessed by the efficiency of amplification of the hprt gene (upper primer, 5′-TCTTTGCTGACCTGCTGGATT-3′, corresponding to bases 222–241; lower, 5′-TATGTCCCCCGTTGACTGATC-3′, corresponding to bases 322–342, GenBank accession no. NM-013556). PCR amplification was then performed with specific primers for PAC1, VPAC1, VPAC2, PACAP, and VIP, for which primers were designed using Primer Express software (Perkin-Elmer, Torrance, CA), as follows. PAC1: upper, 5′-CTTCGATGCTTGTGGGTTTGA-3′, corresponding to bases 543–563 and lower, 5′-AAGCGGCACAAGATGACCAT-3′, bases 667–686, GenBank accession no. D82935; VPAC1: upper, 5′-TCCCCCATTCACGGCTATAA-3′, bases 413–423, and lower, 5′-CAGTCTGTTGCTGCTCATCCAT-3′, bases 525–540, GenBank accession no. NM011703; VPAC2: upper, 5′-CTTCTCCAGATGTTGGTGGCA-3′, bases 981–1,001, and lower, 5′-CCAATAGGGAAGGCAGCAAAC-3′, bases 1,078–1,098, GenBank accession no. D28132; PACAP: upper, 5′-GGCATGTGGGACAATATCACAT-3′, bases 319–340, and lower, 5′-ACTTGGTCCGGGTTGAAGATC-3′, bases 399–419, GenBank accession no. NM009625; VIP: upper, 5′-GGAACAGACTGGTGGAGCCTT-3′, bases 55–75, and lower, 5′-TTCCATCTCGGTGCCTCCT-3′, bases 152–170, GenBank accession no. NM011702. To determine the expression of PAC1 splice variants, we used primer pairs and the condition of PCR amplification described previously (Jamen et al., 2002). A scheme for the design of primers for PAC1 splice variants is shown in Fig. 5A. For short or hip-hop variants: upper, 5′-CATCCTTGTGCAGAAGCTGC-3′, corresponding to bases 1,456–1,475, and lower, 5′-GGTGCTTGAAGTCCATAGTG-3′, bases 1,825–1,844; hip variants: upper, 5′-ACAAATTTAAGACTGAGAGT-3′, bases 1,456–1,475, and lower, 5′-GGTGCTTGAAGTCCATAGTG-3′, bases 1,825–1,844. PCR was performed with an initial step at 94°C for 5 min followed by 35 cycles of 94°C for 30 s, 55°C for 30 s, 72°C for 1 min, and then a final cycle of 72°C for 10 min. Amplification products were stored at 4°C and then electrophoresed on a 2% agarose gel; the bands were visualized by ethidium bromide staining.

Immunohistochemistry and Immunocytochemistry

On embryonic day 14.5, C57BL/6J mouse brains were removed and fixed with 4% paraformaldehyde (PFA) for 8 h, cryoprotected in 20% sucrose in PBS, and frozen. Twenty-micrometer-thick coronal sections were cut with a cryostat, placed on APS-coated glass slides and then fixed with 4% PFA, washed three times with PBS, permeabilized with 0.1% (w/v) Triton X-100/PBS for 5 min and finally washed three times with PBS. Fixed sections were incubated for 30 min with 3% bovine serum albumin (Sigma). Sections were incubated overnight at 4°C with diluted primary polyclonal anti-PAC1 (1:1,000), see earlier for manufacturer's details, anti-PACAP38 (1:1,000) and anti-nestin (1:500) for triple staining. These sections were incubated for 1 h with diluted secondary antibodies (goat anti-mouse Alexa Fluor 633, goat anti-rabbit Alexa Fluor 488, and rabbit anti-goat Alexa Fluor 594) and washed with PBS. Confocal microscopy was performed using the Leica TCS SP2 spectral confocal scanning system (Leica Microsystems). For immunofluorescence measurements, cultured mouse embryonic NPCs were grown on poly-L-ornithine- and fibronectin-coated dishes. All incubations and washes were performed at room temperature. Cells were fixed with 4% PFA, washed three times with PBS, permeabilized with 0.1% Triton X-100/PBS for 5 min and then washed three times with PBS. Fixed cells were incubated for 30 min with 3.3% goat or rabbit serum (Nichirei, Tokyo, Japan). Cells were incubated for 0.5–1 h with diluted primary polyclonal or monoclonal antibody (both were used for double-staining). Next, these cells were incubated for 0.5–1 h with diluted secondary antibodies conjugated to fluorescein and washed with PBS. For BrdU labeling, cells were incubated with 2 M HCl at 37°C for 30 min, rinsed in 0.1 M sodium borate buffer and processed for immunocytochemistry. As a negative control in immunohistochemistry and immunocytochemistry, we performed the omission of either primary or secondary antibodies. Confocal microscopy was performed using the FLUOVIEW confocal microscope system (Olympus, Tokyo, Japan).

[^{3}H]Thymidine Incorporation Assay

Cortical embryonic NPCs were seeded in 96-well plates (1×10^4 cells/well) in 100 μL of medium and cultured for 24 h at 37°C with b-FGF (5 ng/mL). Vehicle or peptide (PACAP38, 0–100 nM; maxadilan, 0–10 nM; or M65, 10 nM) was then added; after 1 h, 1 μCi/well [^{3}H]thymidine was also added. After a 7-h incubation, the cells were washed extensively with medium, and [^{3}H]thymidine incorporation was measured using a β-counter.

For the CM proliferation assay, embryonic cortical NPCs were seeded in 96-well plates (1×10^4 cells/well) in 100 μL of medium and cultured for 24 h at 37°C. Medium was then replaced with NPC conditioned medium or control medium. [^{3}H]thymidine incorporation and measurement were performed as described above.

To assess PAC1 signaling, cortical embryonic NPCs were seeded in 96-well plates (10^4 cells/well) in 100 μL of medium and cultured for 24 h at 37°C. Cells were pre-incubated for an additional 1 h with vehicle and signal transduction inhibitors (H89, 10 μM 2-APB, 20 μM; chelerythrine, 50 μM), and then maxadilan (10 nM) was added. [^{3}H]thymidine incorporation was measured as described above.

Intracellular ATP Assays

It has been previously reported that intracellular ATP levels correlate with cell number (Crouch et al., 1993). Embryonic cortical NPCs were seeded in 48-well plates (4.5×10^4 cells/well) in 400 μL of medium and cultured for 24 h at 37°C with b-FGF (5 ng/mL). After 24 h, each peptide (PACAP38, 0–100 nM; maxadilan, 0–10 nM; PACAP(6–38), 10 nM) was added to these NPC cultures. After a 6 or 24-h incubation with the peptides, intracellular ATP levels were measured using the CellTiter-Glo Luminescent Cell Viability Assay kit (Promega, Madison, WI) according to the manufacturer's instructions.

Radioimmunoassay for PACAP38

PACAP38 concentration was measured in conditioned medium derived from NPCs using a radioimmunoassay (RIA). Cell-free conditioned medium (100 μL) and conditioned medium derived from NPCs (100 μL) were incubated with polyclonal anti-PACAP38, which was rehydrated in RIA buffer (Phoenix Pharmaceuticals, Belmont, CA) for 24 h at 4°C. These reactions were incubated with ^{125}I-PACAP(31–38) (50 cpm/μL) for an additional 24 h at 4°C. Second antibody reaction/separation and detection of ^{125}I in the pellets were performed in a scintillation well gamma counter according to the instrument manufacturer's instructions (Phoenix Pharmaceuticals, Belmont, CA).

Intracellular cAMP Measurement

Cortical embryonic NPCs were seeded in 96-well plates and treated with PACAP38 (100 nM) or maxadilan (10 nM) for 24 h. cAMP levels were assayed by the cAMP-Screen™ System (Applied Biosystems).

Intracellular Calcium Imaging

Cortical embryonic NPCs were seeded in 96-well plates and cultured for 24 h as described above for the intracellular cAMP measurement. The intracellular concentration of free calcium ($[Ca^{2+}]i$) in cultured NPCs was monitored using the Calcium Kit-Fluo 3 (Dojindo Laboratories, Kumamoto, Japan) according to the manufacturer's instructions. For a negative control, cells were pre-incubated for an additional 1 h with BAPTA-AM (100 μM), and then PACAP38 (100 nM) or maxadilan (10 nM) was added.

RESULTS

Expression of PAC1 and PACAP in Embryonic Cortical NPCs In Vivo and In Vitro

To generate a highly purified population of embryonic cortical NPCs, we prepared a secondary culture of NPCs (Li et al., 2001; Nakashima et al., 1999). Most of these cells were positive for nestin, a specific marker for NPCs in developmental brain, but less than 0.5% were immunoreactive for β III tubulin and GFAP. Gal C positive cells were not found (data not shown).

We used RT-PCR and immunohistochemical methods to investigate PAC1 and PACAP expression in cultured mouse embryonic cortical NPCs. RT-PCR detected both PAC1 and PACAP mRNAs in the NPCs and mouse telencephalon at embryonic day 14.5 (Fig. 1A). Other PACAP receptors, VPAC1 and VPAC2, mRNAs were expressed at a much lower level [(0.01 ± 1.7)% and (0.11 ± 2.3)% (mean ± S.E.M.), respectively] than PAC1 mRNA (33.1 ± 0.23)% (Fig. 1A). In addition, the mRNA for another PAC1 ligand, VIP, was not detected in embryonic cortical NPCs (Fig. 1A). In immunohistochemistry experiments, PACAP protein was expressed in nestin-immunoreactive NPCs, and most nestin-immunoreactive NPCs expressing PAC1 colocalized with PACAP in the VZ and SVZ (Fig. 1B). We also detected PACAP and PAC1 in nestin-immunoreactive cultured embryonic cortical NPCs. Over 99.8% of the PAC1-expressing cells co-expressed PACAP (Fig. 1C).

Activation of PAC1 Signaling Induces Embryonic Cortical NPC Proliferation in the Presence of b-FGF in an Autocrine Manner

We performed a [^{3}H]thymidine incorporation assay and an ATP assay, which measures intracellular ATP

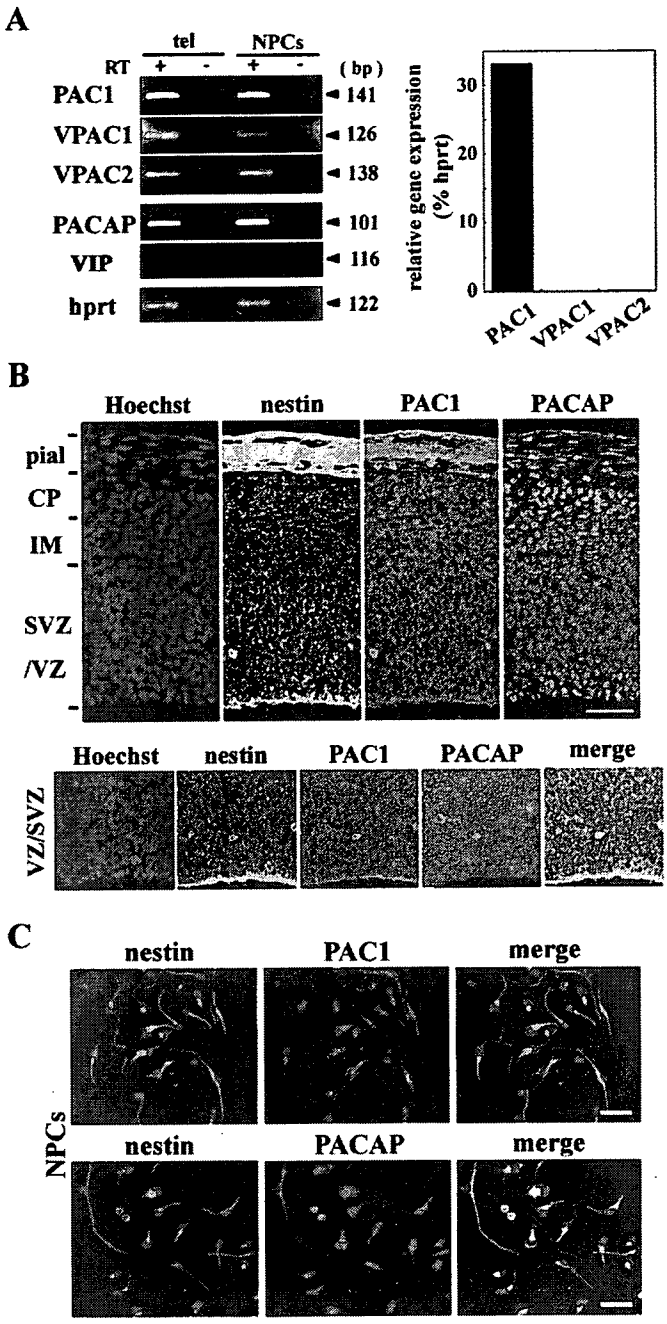

Fig. 1. NPCs express the PACAP receptors PAC1, VPAC1 and VPAC2, and their ligand, PACAP. **A:** RT-PCR was performed as described in Material and Methods. PCR products corresponding to these receptor and ligand genes were loaded onto a 3% agarose gel, as indicated at the left. The size of the PCR products is indicated on the right. Quantitative analysis of mRNA transcripts for PACAP receptors in NPCs by SYBER green-based PCR 7700 system. Data represents expression level of individual PACAP receptors relative to the expression level of hprt. **B,C:** PACAP is an autocrine factor of NPCs. PAC1 and PACAP protein expression was determined by immunofluorescence in vivo (B) and in vitro (C). Nestin-immunoreactive cells (cyan) in E14.5 mouse embryonic telencephalon also expressed PAC1 (green) and PACAP (red). The lower panels are high magnifications of the upper panels (B). Cell nuclei were counterstained with Hoechst 33258 (blue, B). Almost all nestin-immunoreactive NPCs (red, C) expressed PAC1 (green, top panel in C) and PACAP (green, lower panel in C). Cell nuclei were counterstained with Hoechst 33258 (blue, C). Scale bars: (B, C) 50 μm.

levels and hence indicates the viable cell number, to determine whether PAC1 signaling promotes NPC proliferation. A 6-h incubation neither with PACAP38 (0–100 nM), the natural ligand for PAC1, nor with maxadilan (0–1 nM), a specific agonist for PAC1, induced DNA synthesis in the absence of b-FGF (Fig. 2A). In contrast, both reagents increased [^{3}H]thymidine incorporation in a dose-dependent manner in the presence of b-FGF without altering the viable cell number as assessed by the ATP assay (Figs. 2A,B). After incubation for 24 h, maxadilan increased intracellular ATP levels in the presence of b-FGF, and this increase was completely inhibited by the PAC1-specific antagonist, PACAP(6–38) (Fig. 2C). The PAC1 ligand, VIP, also increased [^{3}H]thymidine incorporation in NPCs (Fig. 2D) after incubation for 6 h. However, the DNA synthesis-promoting activity of VIP was lower than that of PACAP38 or maxadilan, and was inhibited by PACAP(6–38) (data not shown). These results indicate that activation of PAC1 promotes DNA synthesis in 6 h followed by NPC proliferation in 24 h in cultures supplemented with b-FGF.

To investigate whether PACAP secreted from embryonic cortical NPCs induces DNA synthesis in the presence of b-FGF, we analyzed [^{3}H]thymidine incorporation in NPCs cultured with conditioned medium derived from embryonic cortical NPCs supplemented with b-FGF. After 7 h, [^{3}H]thymidine incorporation increased by 140% relative to NPCs cultured with NPC-free media, and this activity was inhibited by another PAC1-specific antagonist, M65 (Fig. 3). Similar inhibition was observed when PACAP(6–38) was used (data not shown). We also performed a radioimmunoassay to detect PACAP38 in the conditioned medium derived from NPCs. The PACAP concentration was substantially higher in conditioned medium derived from NPCs (284 ± 2.3 pg/mL, Mean ± SEM) than in NPC-free medium (0.072 ± 0.25 pg/mL, Mean ± SEM).

PLC/IP$_3$ Signaling Pathway are Activated by Maxadilan Via PAC1 Splice Variants in Embryonic Cortical NPCs

To determine which splice variant (or variants) was expressed in our embryonic cortical NPCs, we performed RT-PCR using splice variant-specific primer pairs. We detected four PAC1 variants (Fig. 4).

To determine whether PAC1 couples to the cAMP pathway, we measured intracellular cAMP concentration in NPCs after treatment with PACAP38 or maxadilan. Both reagents elicited a 3.5–4-fold increase in intracellular cAMP concentration (Fig. 5A). We used the Fluo-3 ratio method to determine the effects of PAC1 activation on calcium signaling. The intracellular calcium level ([Ca^{2+}]i) increased rapidly in NPCs following treatment with PACAP38 or maxadilan (Fig. 5B). This activity was inhibited by BAPTA-AM, which was an intracellular Ca^{2+}-chelator (Fig. 5B). We used pathway-specific in-

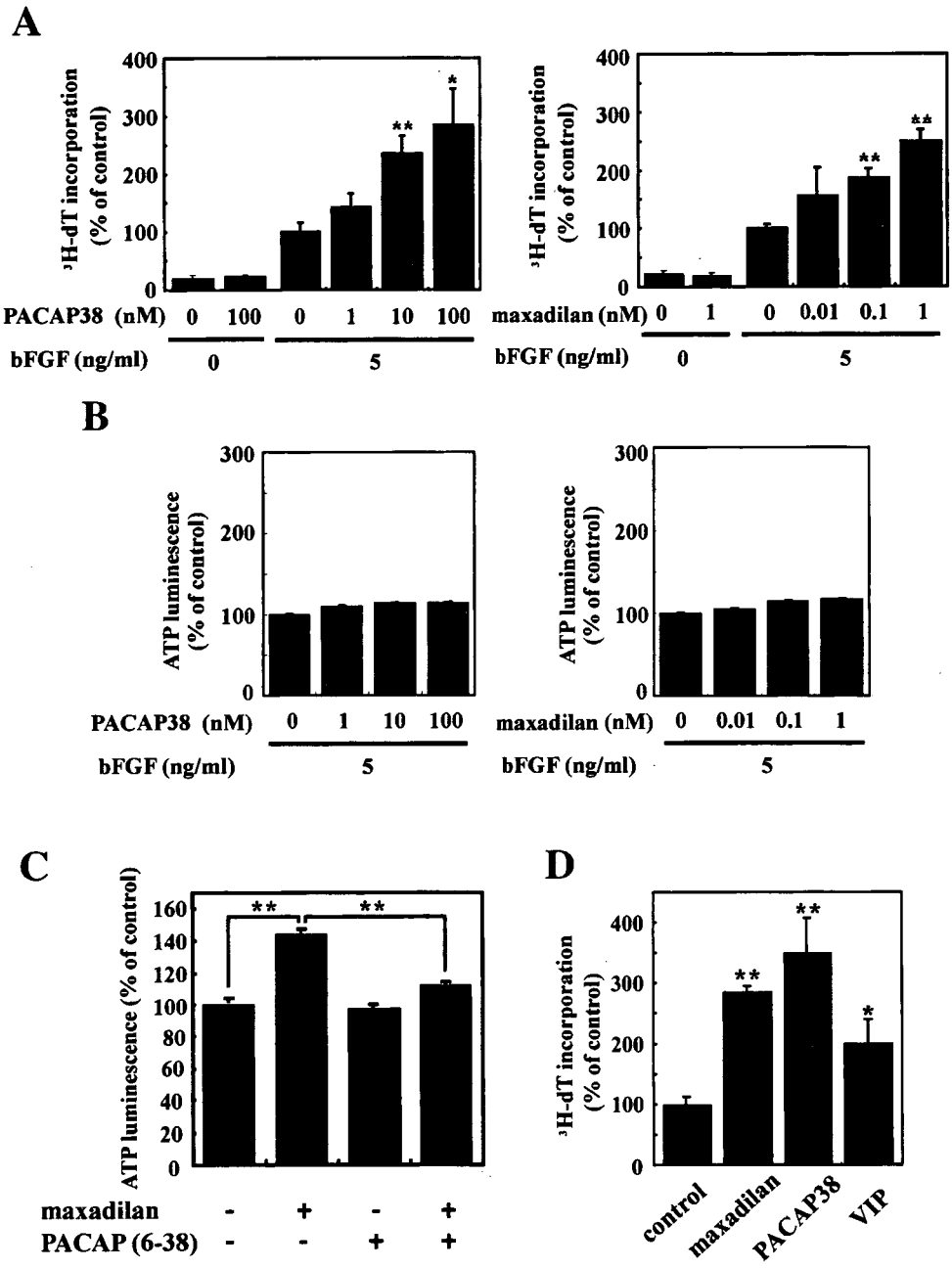

Fig. 2. PAC1 signaling promotes NPC growth in the presence of b-FGF. **A,B:** PACAP38 and maxadilan promote DNA synthesis and cell growth of NPCs in a dose-dependent manner in the presence of b-FGF. NPCs were cultured with PACAP38 (0–100 nM) (left) or maxadilan (0–1 nM) (right) in the presence or absence of b-FGF (5 ng/mL) for 7 h, and then [^{3}H]thymidine was added during the last 6 h of culture (A). NPCs were cultured with PACAP38 (left) or maxadilan (right) in the presence of b-FGF (5 ng/mL) for 6 h, and then the growth rate was examined by an ATP luminescence assay (B). **C:** The PAC1-specific agonist, maxadilan, promotes NPC growth; blockade of PAC1 with the PAC1-specific antagonist, PACAP (6–38), completely cancels this growth-promoting activity. NPCs were incubated with or without maxadilan (1 nM) for 24 h. Maxadilan-induced cell growth was inhibited by co-incubation with PACAP (6–38) (10 nM). **D:** NPCs were cultured with or without PACAP38 (100 nM), maxadilan (10 nM) or VIP (1 μM) in the presence of b-FGF for 7 h, and then [^{3}H]thymidine was added during the last 6 h of culture. Bars represent mean ± SD (n = 4). Significant differences from control (without agonist or antagonist) are indicated by asterisks (*P < 0.05; **P < 0.01, ANOVA).

hibitors for protein kinase A (PKA) or inositol 1,4,5-trisphosphate (IP3)/C kinase (PKC) to determine which signaling pathway mediates PAC1 activity during embryonic cortical NPC proliferation. H89, which inhibits cAMP-dependent PKA, did not inhibit the maxadilan-induced increase in [^{3}H]thymidine incorporation; however, 2-APB, which inhibits the IP3 receptor, had a strong inhibitory effect (Fig. 5C). In addition, chelerythrin, which inhibits PKC, did not inhibit the effect of maxadilan. Taken together, these results indicate that NPC proliferation involved the PLC/IP_3-dependent signaling pathway and a downstream Ca^{2+}-dependent pathway.

PAC1 Activation Induces NPC Proliferation and Morphological Changes in Embryonic Cortical NPCs

Upon maxadilan stimulation for 48 h, we observed a morphological change, which was an elongation of cell processes with stellate and astrocyte-like morphology, in nestin-immunoreactive NPCs (Fig. 6A). To determine the relationship between NPC proliferation and the morphological changes seen by PAC1 signaling, we identified nestin-immunoreactive NPCs in the mitotic phase with a BrdU incorporation assay. Immediately after 10 min of

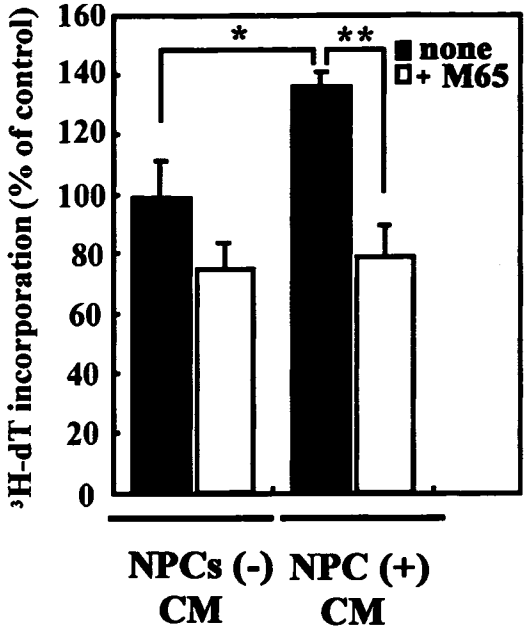

Fig. 3. The activation of PAC1-induced NPC proliferation in autocrine system. NPCs were cultured for 24 h, and the conditioned medium (CM) was collected. The CM or control cell-free media was added to freshly prepared NPC cultures and incubated for 7 h. [^{3}H]thymidine was added during the last 6 h, and incorporation was later measured. DNA synthesis-promoting activity in CM was observed and this activity was inhibited by the PAC1-selective antagonist, M65 (10 nM). Bars represent mean ± SD (n = 4). Significant differences from the control are indicated by asterisks (*P < 0.05, **P < 0.01; ANOVA).

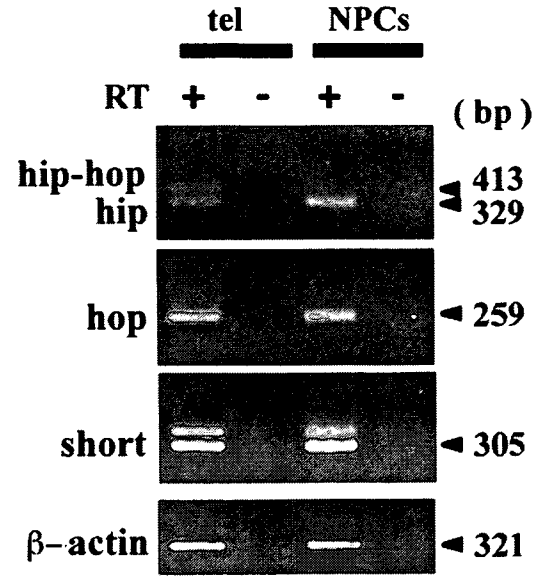

Fig. 4. NPCs express all PAC1 isoforms. RT-PCR was performed as described in Material and Methods. RT-PCR of E14.5 mouse embryonic telencephalon (tel) was used for comparison. The PCR products corresponding to the PAC1 isoforms were loaded onto a 3% agarose gel, as indicated at the left. The size of the PCR products is indicated on the right.

exposure to BrdU, the unincorporated BrdU was washed off the NPCs and maxadilan (10 nM) was added in BrdU-free and b-FGF contained medium. After 24 h, maxadilan increased the number of BrdU/nestin immunoreactive NPCs with long cell processes compared with non-treated NPCs (Fig. 6B). Next, we addressed the differentiation of BrdU immunoreactive NPCs to neurons, astrocytes, or oligodendrocytes. We observed a gradual increase of BrdU immunoreactive NPCs by the 24-h treatment of maxadilan during 7 days, compared with non-treated NPCs. The treatment of maxadilan did not increase the number of β III tubulin immunoreactive neurons, whereas maxadilan induced marked increase of GFAP immunoreactive astrocytes. Moreover, we observed the significant increase in the percentage of BrdU/GFAP double immunoreactive astrocytes, compared with that of non-treated NPCs at day 7 (Figs. 6B–E). These data suggested that PAC1 signaling regulates the proliferation of glial progenitor cells to generate astrocytes in E14.5 NPCs.

DISCUSSION

The PACAP/PAC1 system plays an important role in regulating differentiation of embryonic NPCs at E12–17 (Lee et al., 2001; Lelievre et al., 2002; Lu and DiCicco-Bloom, 1997; Lu et al., 1998; Suh et al., 2001). In our results, the PACAP/PAC1 autocrine system potentiated growth factor-promoted proliferation of E14.5 mouse cortical NPCs. Moreover, we found that the activation of PAC1 initiated morphological changes, which were cell process elongation of typical astrocytes in embryonic cortical NPCs. In the BrdU incorporation assay, most of BrdU positive NPCs differentiated to astrocytes. We suggest dual aspects of PAC1 signaling in the regulation of not only differentiation but also proliferation of NPCs at E14.5 via PLC/IP_3 signaling pathways through PAC1 variants in NPCs committed to an astrocytic lineage.

We found that the PACAP/PAC1 system potentiated growth factor-induced proliferation of E14.5 mouse cortical NPCs in an autocrine manner. Many trophic factor-generated microenvironments control NPC proliferation or differentiation. In particular, growth factors such as b-FGF, EGF, and TGFα promote NPC proliferation in the embryonic and postnatal brain (Gritti et al., 1996; Kilpatrick and Bartlett, 1993; Richards et al., 1992; Vescovi et al., 1999). Although these growth factors are soluble and thus diffuse widely in the CNS, their regulation during development has not been fully understood. In our results, immunoreactivity for PACAP and PAC1 in VZ/SVZ as well as the detection of PACAP38 in conditioned medium derived from NPCs supported the evidence of a PACAP/PAC1 autocrine loop in embryonic NPCs. Several molecules function in an autocrine manner in embryonic NPCs. BMPs and noggin are autocrine factors that regulate NPC proliferation and differentiation (Mabie et al., 1999; Nadarajah et al., 2002; Panchision et al., 2001; Sauvageot and Stiles, 2002). In adult brain, Cystatin C, IGF-I and stem cell-derived stem/progenitor cell-supporting factor have been charac-

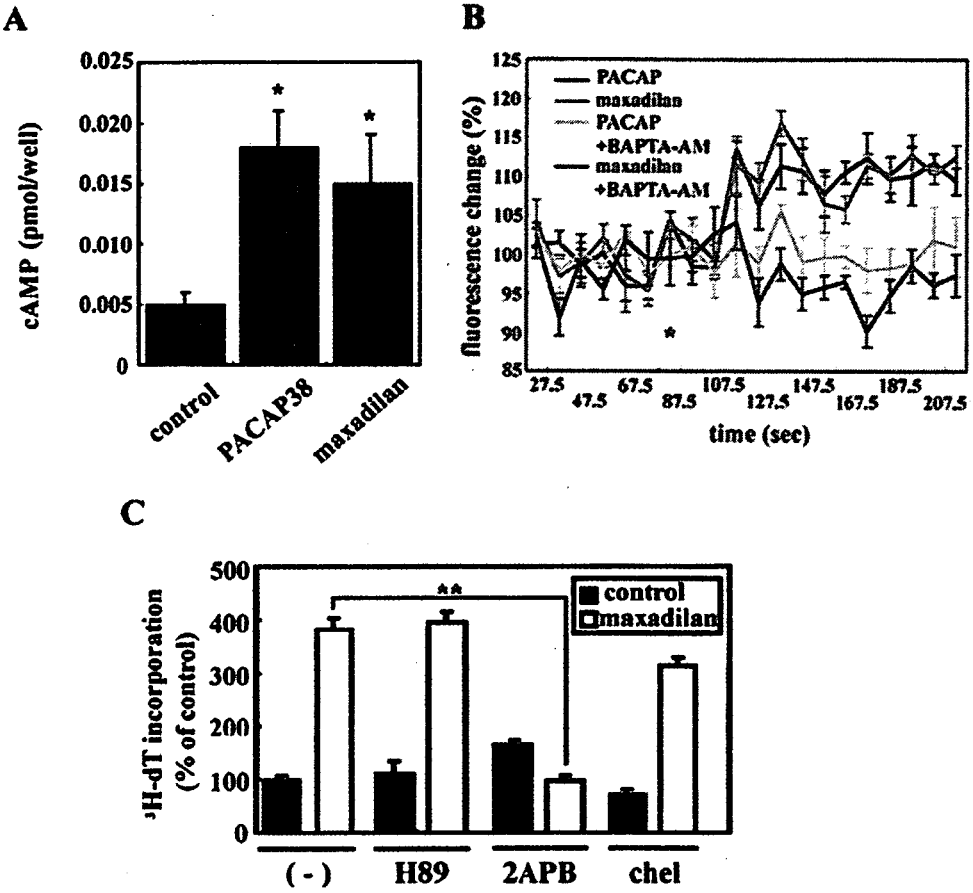

Fig. 5. PACAP promotes DNA synthesis in NPCs via PKC and IP3, but the PAC1-selective agonist, maxadilan, promotes the activity via IP3 only. **A:** The activation of PAC1 increases intracellular cAMP level in NPCs. The intracellular cAMP content in NPCs was measured after treatment with PACAP38 (100 nM) or maxadilan (10 nM) for 15 min by ELISA system. **B:** The activation of PAC1 increases intracellular calcium level ($[Ca^{2+}]i$) in NPCs. The ratio of ($[Ca^{2+}]i$ was analyzed by Fluo-3 AM imaging at the steady state and after the treatment* of PACAP38 (100 nM) or maxadilan (10 nM). **C:** NPCs were incubated with 10 μM H89, 2.5 μM 2-APB or 100 nM chelerythrine in the presence of 5 ng/mL b-FGF for 1 h before the addition of 100 nM PACAP38 or 10 nM maxadilan. [^{3}H]thymidine was added during the last 6 h of culture. Data represent mean values ± SD (n = 4). Significant differences from the control are indicated by asterisks (*P < 0.05, **P < 0.01; ANOVA).

terized as autocrine/paracrine growth-supporting factors for adult NPC proliferation, which is promoted by b-FGF/EGF (Toda et al., 2003). These factors are required to maintain multipotent adult NPC proliferation (Toda et al., 2003). These autocrine systems, including the PACAP/PAC1 system, are considered to play an important role in restricting or amplifying growth factor-mediated signals and in controlling NPC proliferation and differentiation.

At an early developmental stage (E12–14) during which the mouse cortex undergoes neurogenesis, the PACAP/PAC1 system promotes neuronal differentiation of cortical NPCs (Dicicco-Bloom et al., 1998; Lee et al., 2001; Lu and DiCicco-Bloom, 1997; Suh et al., 2001). In contrast, cortical NPCs derived from a late stage (E17) promote astrocyte differentiation via PAC1 (Vallejo and Vallejo, 2002). Furthermore, at the postnatal stage, when oligogenesis occurs, PAC1 signaling regulates both the growth and differentiation of oligodendrocyte progenitor cells (Lee et al., 2001). Thus the PACAP/PAC1 system plays multiple roles in the different cell lineages during development, and this fact suggests that it may function via several signaling pathways. Recent studies have shown that Gs- or Gq-mediated intracellular signal via PAC1 splice variants induced a specific biological activity, differentiation or proliferation, in cortical progenitor cells (Bresson-Bepoldin et al., 1998; Jaworski and Proctor, 2000; Lu et al., 1998; Zhou et al., 2000a,b). Our RT-PCR experiment showed that PAC1 splice variants were expressed in mouse embryonic cortical NPCs at E14.5. Moreover, we detected intracellular cAMP accumulation and $[Ca^{2+}]i$ increase via PAC1 activation in NPCs (Figs. 5A,B). These results suggested that the activation of PAC1 stimulated both Gs-mediated AC/PKA and Gq-mediated PLC/IP3 signaling pathways in embryonic cortical NPCs at E14.5 via PAC1 variants. Although many studies have reported that AC/PKA signal induced NPC differentiation into neuron or glial cells via PAC1 (Zhou et al., 2001), the effects of PLC/IP3 signal in NPC lineage is unknown. We found that IP3 inhibitor curtailed PAC1-mediated NPC proliferation (Fig. 5C), suggesting that Gq-mediated PLC/IP3, not Gs-mediated AC/PKA, signaling pathway modulated NPC proliferation via the PAC1 variant which might give rise to different signaling pathways for NPC differentiation and proliferation.

Cortical NPCs at E14.5 may have heterogeneous subpopulations. Some of these are multipotent and others are committed to neuronal or glial progenitors which generate neurons or astrocytes (Sauvageot and Stiles, 2002). As indicated by our morphological study and BrdU labeling, PAC1 signaling potentiated the pro-

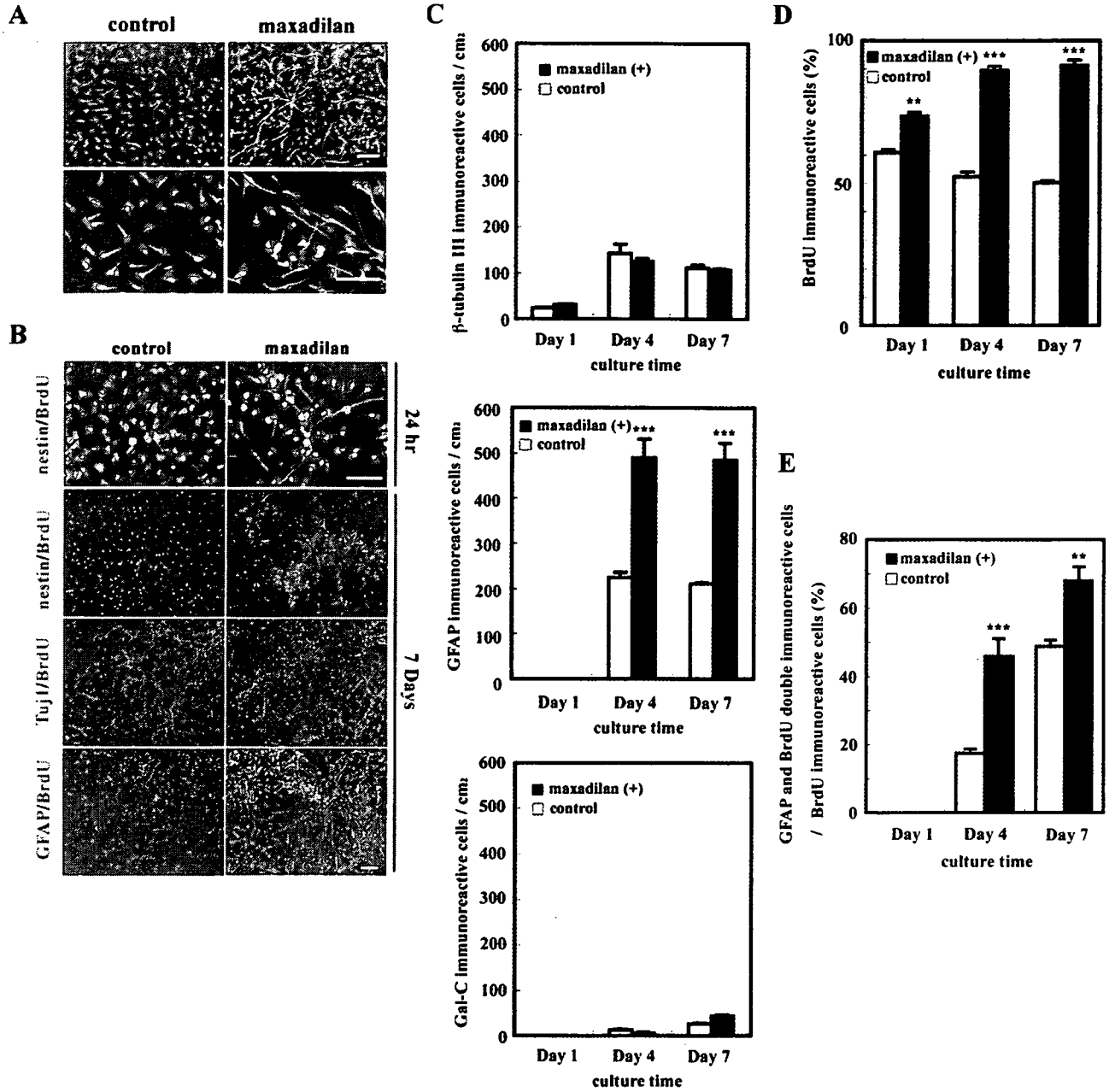

Fig. 6. PAC1 signaling promotes the proliferation of embryonic cortical NPCs committed to astrocytes. **A:** After maxadilan treatment for 24 h, cells were fixed and stained for nestin (green), Hoechst (blue) and BrdU (red). **B:** After maxadilan treatment for 7 days, cells were fixed and stained for nestin (green), β III tubulin (b III tub) (green), GFAP (green), Hoechst (blue) and BrdU (red). **C:** Quantitative analysis of differentiation of embryonic cortical NPCs treated or non-treated with maxadilan for 7 days. **D:** Proliferation of embryonic cortical NPCs treated or non-treated with maxadilan assessed by BrdU incorporation assay. **E:** Time course of astrogenesis from BrdU immunoreactive embryonic cortical NPCs treated or non-treated with maxadilan. Total cellular counts were obtained as described in Materials and Methods. Data represent mean values ± SD ($n = 4$). Significant differences from the control are indicated by asterisks (*$P < 0.05$, **$P < 0.01$, ***$P < 0.001$; ANOVA). Scale bars: (A, B) 50 μm.

liferation of NPCs with longer cell processes manifesting astrocyte-like shapes. Moreover, most BrdU immunoreactive NPCs were differentiated into GFAP immunoreactive astrocytes via PAC1. One of the autocrine factor families, BMPs, are reported to promote astrocytic differentiation and to change the proliferative activities of cortical NPCs in the different developmental stages (Gross et al., 1996; Mabie et al., 1999). Our data may reflect a dual role for the PACAP/PAC1 system; potentiating glial progenitor cell proliferation and subsequent astrogenesis as well as astrocytic differentiation in NPCs similar to BMPs. The PACAP/PAC1 autocrine system is critical for the regulation of NPC and glial lineage, depending on the stage of brain development.

ACKNOWLEDGMENTS

We thank Dr. Richard G. Titus for providing maxadilan and M65. We thank Mr. Ayukawa K. and Mrs. Hara Y. for the early work contribution and excellent technical help.

REFERENCES

Altman J, Bayer SA. 1990a. Horizontal compartmentation in the germinal matrices and intermediate zone of the embryonic rat cerebral cortex. Exp Neurol 107:36–47.

Altman J, Bayer SA. 1990b. Vertical compartmentation and cellular transformations in the germinal matrices of the embryonic rat cerebral cortex. Exp Neurol 107:23–35.

Arimura A. 1998. Perspectives on pituitary adenylate cyclase activating polypeptide (PACAP) in the neuroendocrine, endocrine, and nervous systems. Jpn J Physiol 48:301–331.

Basille M, Gonzalez BJ, Desrues L, Demas M, Fournier A, Vaudry H. 1995. Pituitary adenylate cyclase-activating polypeptide (PACAP) stimulates adenylyl cyclase and phospholipase C activity in rat cerebellar neuroblasts. J Neurochem 65:1318–1324.

Basille M, Gonzalez BJ, Leroux P, Jeandel L, Fournier A, Vaudry H. 1993. Localization and characterization of PACAP receptors in the rat cerebellum during development: Evidence for a stimulatory effect of PACAP on immature cerebellar granule cells. Neuroscience 57: 329–338.

Bluet-Pajot MT, Epelbaum J, Gourdji D, Hammond C, Kordon C. 1998. Hypothalamic and hypophyseal regulation of growth hormone secretion. Cell Mol Neurobiol 18:101–123.

Bresson-Bepoldin L, Jacquot MC, Schlegel W, Rawlings SR. 1998. Multiple splice variants of the pituitary adenylate cyclase-activating polypeptide type 1 receptor detected by RT-PCR in single rat pituitary cells. J Mol Endocrinol 21:109–120.

Cazillis M, Gonzalez BJ, Billardon C, Lombet A, Fraichard A, Samarut J, Gressens P, Vaudry H, Rostene W. 2004. VIP and PACAP induce selective neuronal differentiation of mouse embryonic stem cells. Eur J Neurosci 19:798–808.

Christophe J. 1993. Type I receptors for PACAP (a neuropeptide even more important than VIP?). Biochim Biophys Acta 1154:183–199.

Crouch SP, Kozlowski R, Slater KJ, Fletcher J. 1993. The use of ATP bioluminescence as a measure of cell proliferation and cytotoxicity. J Immunol Methods 160:81–88.

Dicicco-Bloom E, Lu N, Pintar JE, Zhang J. 1998. The PACAP ligand/receptor system regulates cerebral cortical neurogenesis. Ann N Y Acad Sci 865:274–289.

Eccleston PA, Mirsky R, Jessen KR. 1991. Spontaneous immortalisation of Schwann cells in culture: Short-term cultured Schwann cells secrete growth inhibitory activity. Development 112:33–42.

Gritti A, Parati EA, Cova L, Frolichsthal P, Galli R, Wanke E, Faravelli L, Morassutti DJ, Roisen F, Nickel DD, Vescovi AL. 1996. Multipotential stem cells from the adult mouse brain proliferate and self-renew in response to basic fibroblast growth factor. J Neurosci 16:1091–1100.

Gross RE, Mehler MF, Mabie PC, Zang Z, Santschi L, Kessler JA. 1996. Bone morphogenetic proteins promote astroglial lineage commitment by mammalian subventricular zone progenitor cells. Neuron 17:595–606.

Jamen F, Puech R, Bockaert J, Brabet P, Bertrand G. 2002. Pituitary adenylate cyclase-activating polypeptide receptors mediating insulin secretion in rodent pancreatic islets are coupled to adenylate cyclase but not to PLC. Endocrinology 143:1253–1259.

Jaworski DM, Proctor MD. 2000. Developmental regulation of pituitary adenylate cyclase-activating polypeptide and PAC(1) receptor mRNA expression in the rat central nervous system. Brain Res Dev Brain Res 120:27–39.

Kaufman MH. 1998. The atlas of mouse development. London: Academic press.

Kilpatrick TJ, Bartlett PF. 1993. Cloning and growth of multipotential neural precursors: Requirements for proliferation and differentiation. Neuron 10:255–265.

Lee M, Lelievre V, Zhao P, Torres M, Rodriguez W, Byun JY, Doshi S, Ioffe Y, Gupta G, de los Monteros AE. 2001. Pituitary adenylyl cyclase-activating polypeptide stimulates DNA synthesis but delays maturation of oligodendrocyte progenitors. J Neurosci 21:3849–3859.

Lelievre V, Hu Z, Byun JY, Ioffe Y, Waschek JA. 2002. Fibroblast growth factor-2 converts PACAP growth action on embryonic hindbrain precursors from stimulation to inhibition. J Neurosci Res 67:566–573.

Li BS, Ma W, Zhang L, Barker JL, Stenger DA, Pant HC. 2001. Activation of phosphatidylinositol-3 kinase (PI-3K) and extracellular regulated kinases (Erk1/2) is involved in muscarinic receptor-mediated DNA synthesis in neural progenitor cells. J Neurosci 21:1569–1579.

Liu SY, Zhang ZY, Song YC, Qiu KJ, Zhang KC, An N, Zhou Z, Cai WQ, Yang H. 2004. SVZa neural stem cells differentiate into distinct lineages in response to BMP4. Exp Neurol 190:109–121.

Lu N, DiCicco-Bloom E. 1997. Pituitary adenylate cyclase-activating polypeptide is an autocrine inhibitor of mitosis in cultured cortical precursor cells. Proc Natl Acad Sci USA 94:3357–3362.

Lu N, Zhou R, DiCicco-Bloom E. 1998. Opposing mitogenic regulation by PACAP in sympathetic and cerebral cortical precursors correlates with differential expression of PACAP receptor (PAC1-R) isoforms. J Neurosci Res 53:651–662.

Mabie PC, Mehler MF, Kessler JA. 1999. Multiple roles of bone morphogenetic protein signaling in the regulation of cortical cell number and phenotype. J Neurosci 19:7077–7088.

Mercer A, Ronnholm H, Holmberg J, Lundh H, Heidrich J, Zachrisson O, Ossoinak A, Frisen J, Patrone C. 2004. PACAP promotes neural stem cell proliferation in adult mouse brain. J Neurosci Res 76:205–215.

Muller JM, Lelievre V, Becq-Giraudon L, Meunier AC. 1995. VIP as a cell-growth and differentiation neuromodulator role in neurodevelopment. Mol Neurobiol 10:115–134.

Nadarajah B, Alifragis P, Wong RO, Parnavelas JG. 2002. Ventricle-directed migration in the developing cerebral cortex. Nat Neurosci 5:218–224.

Nakashima K, Yanagisawa M, Arakawa H, Kimura N, Hisatsune T, Kawabata M, Miyazono K, Taga T. 1999. Synergistic signaling in fetal brain by STAT3-Smad1 complex bridged by p300. Science 284: 479–482.

Otto C, Kovalchuk Y, Wolfer DP, Gass P, Martin M, Zuschratter W, Grone HJ, Kellendonk C, Tronche F, Maldonado R. 2001. Impairment of mossy fiber long-term potentiation and associative learning in pituitary adenylate cyclase activating polypeptide type I receptor-deficient mice. J Neurosci 21:5520–5527.

Panchision DM, Pickel JM, Studer L, Lee SH, Turner PA, Hazel TG, McKay RD. 2001. Sequential actions of BMP receptors control neural precursor cell production and fate. Genes Dev 15:2094–2110.

Pisegna JR, Moody TW, Wank SA. 1996. Differential signaling and immediate-early gene activation by four splice variants of the human pituitary adenylate cyclase-activating polypeptide receptor (hPACAP-R). Ann N Y Acad Sci 805:54–64. Discussion 64–66.

Rayan GM, Said SI, Cahill SL, Duke J. 1991. Vasoactive intestinal peptide and nerve regeneration. J Hand Surg [Br] 16:515–518.

Reynolds BA, Weiss S. 1996. Clonal and population analyses demonstrate that an EGF-responsive mammalian embryonic CNS precursor is a stem cell. Dev Biol 175:1–13.

Reynolds BA, Tetzlaff W, Weiss S. 1992. A multipotent EGF-responsive striatal embryonic progenitor cell produces neurons and astrocytes. J Neurosci 12:4565–4574.

Richards LJ, Kilpatrick TJ, Bartlett PF. 1992. De novo generation of neuronal cells from the adult mouse brain. Proc Natl Acad Sci USA 89:8591–8595.

Sauvageot CM, Stiles CD. 2002. Molecular mechanisms controlling cortical gliogenesis. Curr Opin Neurobiol 12:244–249.

Suh J, Lu N, Nicot A, Tatsuno I, DiCicco-Bloom E. 2001. PACAP is an anti-mitogenic signal in developing cerebral cortex. Nat Neurosci 4:123, 124.

Tatsuno I, Somogyvari-Vigh A, Arimura A. 1994. Developmental changes of pituitary adenylate cyclase activating polypeptide (PACAP) and its receptor in the rat brain. Peptides 15:55–60.

Toda H, Tsuji M, Nakano I, Kobuke K, Hayashi T, Kasahara H, Takahashi J, Mizoguchi A, Houtani T, Sugimoto T. 2003. Stem cell-derived neural stem/progenitor cell supporting factor is an autocrine/paracrine survival factor for adult neural stem/progenitor cells. J Biol Chem 278:35491–35500.

Vallejo I, Vallejo M. 2002. Pituitary adenylate cyclase-activating polypeptide induces astrocyte differentiation of precursor cells from developing cerebral cortex. Mol Cell Neurosci 21:671–683.

Vaudry D, Rousselle C, Basille M, Falluel-Morel A, Pamantung TF, Fontaine M, Fournier A, Vaudry H, Gonzalez BJ. 2002. Pituitary adenylate cyclase-activating polypeptide protects rat cerebellar granule neurons against ethanol-induced apoptotic cell death. Proc Natl Acad Sci USA 99:6398–6403.

Vescovi AL, Parati EA, Gritti A, Poulin P, Ferrario M, Wanke E, Frolichsthal-Schoeller P, Cova L, Arcellana-Panlilio M, Colombo A. 1999. Isolation and cloning of multipotential stem cells from the embryonic human CNS, establishment of transplantable human neural stem cell lines by epigenetic stimulation. Exp Neurol 156:71–83.

Waschek JA, Casillas RA, Nguyen TB, DiCicco-Bloom EM, Carpenter EM, Rodriguez WI. 1998. Neural tube expression of pituitary ade-

nylate cyclase-activating peptide (PACAP) and receptor: Potential role in patterning and neurogenesis. Proc Natl Acad Sci USA 95: 9602–9607.

Waschek JA, Dicicco-Bloom EM, Lelievre V, Zhou X, Hu Z. 2000. PACAP action in nervous system development, regeneration, and neuroblastoma cell proliferation. Ann N Y Acad Sci 921:129–136.

Wislet-Gendebien S, Bruyere F, Hans G, Leprince P, Moonen G, Rogister B. 2004. Nestin-positive mesenchymal stem cells favour the astroglial lineage in neural progenitors and stem cells by releasing active BMP4. BMC Neurosci 5:33.

Zhou C, Kikuyama S, Nakajo S, Hirabayashi T, Mizushima H, Shioda S. 2000a. Splice variants of PAC(1) receptor during early neural development of rats. Peptides 21:1177–1183.

Zhou CJ, Kikuyama S, Shibanuma M, Hirabayashi T, Nakajo S, Arimura A, Shioda S. 2000b. Cellular distribution of the splice variants of the receptor for pituitary adenylate cyclase-activatinsg polypeptide (PAC(1)-R) in the rat brain by in situ RT-PCR. Brain Res Mol Brain Res 75:150–158.

Zhou CJ, Shioda S, Yada T, Inagaki N, Pleasure SJ, Kikuyama S. 2002. PACAP and its receptors exert pleiotropic effects in the nervous system by activating multiple signaling pathways. Curr Protein Pept Sci 3:423–439.

Zhou CJ, Yada T, Kohno D, Kikuyama S, Suzuki R, Mizushima H, Shioda S. 2001. PACAP activates PKA, PKC and Ca(2+) signaling cascades in rat neuroepithelial cells. Peptides 22:1111–1117.